



# Evolution of the Toarcian (Early Jurassic) carbon-cycle and global climatic controls on local sedimentary processes (Cardigan Bay Basin, UK)

Weimu Xu<sup>a,\*</sup>, Micha Ruhl<sup>a</sup>, Hugh C. Jenkyns<sup>a</sup>, Melanie J. Leng<sup>b,c</sup>, Jennifer M. Huggett<sup>d</sup>, Daniel Minisini<sup>e</sup>, Clemens V. Ullmann<sup>f</sup>, James B. Riding<sup>b</sup>, Johan W.H. Weijers<sup>g</sup>, Marisa S. Storm<sup>a</sup>, Lawrence M.E. Percival<sup>a,h</sup>, Nicholas J. Tosca<sup>a</sup>, Erdem F. Idiz<sup>a</sup>, Erik W. Tegelaar<sup>g</sup>, Stephen P. Hesselbo<sup>f,\*</sup>

<sup>a</sup> Department of Earth Sciences, University of Oxford, Oxford OX1 3AN, UK

<sup>b</sup> British Geological Survey, Keyworth, Nottingham NG12 5GG, UK

<sup>c</sup> School of Biosciences, Sutton Bonington Campus, University of Nottingham, Loughborough LE12 5RD, UK

<sup>d</sup> Department of Mineralogy, the Natural History Museum, Cromwell Road, London SW7 5BD, UK

<sup>e</sup> Shell Technological Center, Houston, 3333 South HW6, 77082 Houston, TX, USA

<sup>f</sup> Camborne School of Mines and Environment and Sustainability Institute, University of Exeter, Penryn TR10 9FE, UK

<sup>g</sup> Shell Global Solutions International B.V., Shell Technology Centre Amsterdam, Grasweg 31, 1031 HW, Amsterdam, The Netherlands

<sup>h</sup> Institut des sciences de la Terre, Géopolis, Université de Lausanne, 1015 Lausanne, Switzerland

## ARTICLE INFO

### Article history:

Received 14 May 2017

Received in revised form 12 December 2017

Accepted 16 December 2017

Available online xxxx

Editor: M. Frank

### Keywords:

carbon-isotope stratigraphy

global weathering rates

gravity-flow deposits

oceanic anoxic event (OAE)

siderite

Toarcian (Early Jurassic)

## ABSTRACT

The late Early Jurassic Toarcian Stage represents the warmest interval of the Jurassic Period, with an abrupt rise in global temperatures of up to  $\sim 7^\circ\text{C}$  in mid-latitudes at the onset of the early Toarcian Oceanic Anoxic Event (T-OAE;  $\sim 183$  Ma). The T-OAE, which has been extensively studied in marine and continental successions from both hemispheres, was marked by the widespread expansion of anoxic and euxinic waters, geographically extensive deposition of organic-rich black shales, and climatic and environmental perturbations. Climatic and environmental processes following the T-OAE are, however, poorly known, largely due to a lack of study of stratigraphically well-constrained and complete sedimentary archives. Here, we present integrated geochemical and physical proxy data (high-resolution carbon-isotope data ( $\delta^{13}\text{C}$ ), bulk and molecular organic geochemistry, inorganic petrology, mineral characterisation, and major- and trace-element concentrations) from the biostratigraphically complete and expanded entire Toarcian succession in the Llanbedr (Mochras Farm) Borehole, Cardigan Bay Basin, Wales, UK. With these data, we (1) construct the first high-resolution biostratigraphically calibrated chemostratigraphic reference record for nearly the complete Toarcian Stage, (2) establish palaeoceanographic and depositional conditions in the Cardigan Bay Basin, (3) show that the T-OAE in the hemipelagic Cardigan Bay Basin was marked by the occurrence of gravity-flow deposits that were likely linked to globally enhanced sediment fluxes to continental margins and deeper marine (shelf) basins, and (4) explore how early Toarcian (*tenuicostatum* and *serpentinum* zones) siderite formation in the Cardigan Bay Basin may have been linked to low global oceanic sulphate concentrations and elevated supply of iron (Fe) from the hinterland, in response to climatically induced changes in hydrological cycling, global weathering rates and large-scale sulphide and evaporite deposition.

© 2017 The Authors. Published by Elsevier B.V. This is an open access article under the CC BY license (<http://creativecommons.org/licenses/by/4.0/>).

## 1. Introduction

The Toarcian Stage ( $\sim 183$ – $174$  Ma) is considered to have been the warmest interval of the Jurassic Period encompassing a tran-

\* Corresponding authors.

E-mail addresses: [weimu.xu@earth.ox.ac.uk](mailto:weimu.xu@earth.ox.ac.uk) (W. Xu), [s.p.hesselbo@exeter.ac.uk](mailto:s.p.hesselbo@exeter.ac.uk) (S.P. Hesselbo).

<https://doi.org/10.1016/j.epsl.2017.12.037>

0012-821X/© 2017 The Authors. Published by Elsevier B.V. This is an open access article under the CC BY license (<http://creativecommons.org/licenses/by/4.0/>).

sient temperature rise of up to  $\sim 7^\circ\text{C}$  in mid-latitudes (Dera et al., 2011a; Gradstein et al., 2012; Korte et al., 2015). The stage is also marked by one of the most intense and geographically widespread developments of anoxic/euxinic oceanic conditions of the Mesozoic Era (Jenkyns, 2010). This phenomenon of extreme redox changes is therefore termed the Toarcian Oceanic Anoxic Event (T-OAE, at  $\sim 183$  Ma) and is marked by large-scale organic-carbon burial in shelf-sea settings, deeper marine basins, and lakes

(Jenkyns, 1985, 1988; Xu et al., 2017). The T-OAE was characterised by a severe perturbation to the global carbon cycle, likely associated with the release of volcanogenic CO<sub>2</sub> from the emplacement of the Karoo–Ferrar large igneous province (LIP), and/or thermogenic methane (CH<sub>4</sub>) from sill intrusion into Gondwanan coal and organic-rich shale, and/or biogenic methane from dissociation of sub-seafloor methane clathrates (Duncan et al., 1997; Hesselbo et al., 2000; Kemp et al., 2005; McElwain et al., 2005; Svensen et al., 2007, 2012; Burgess et al., 2015; Percival et al., 2015). The observed early Toarcian carbon-cycle perturbation is thought to have induced a wetter climate in mid latitudes with an accelerated hydrological cycle that caused an increase in silicate weathering on the continents, and subsequent enhanced fluvial delivery of nutrients to the oceans and large inland lakes (Jenkyns et al., 2002; Cohen et al., 2004; Jenkyns, 2010; Dera et al., 2011a; Kemp et al., 2011; Brazier et al., 2015; Percival et al., 2016; Xu et al., 2017; Izumi et al., 2018). Elevated nutrient fluxes are credited with causing increases in primary productivity in the oceans and large lakes and the burial of organic matter in these reservoirs, aided by local water-column stratification. Organic-carbon burial, together with the increase in silicate weathering, ultimately drew down CO<sub>2</sub>, ushering in an inverse greenhouse effect and global cooling (Schouten et al., 2000; Cohen et al., 2004). There is evidence, particularly in northern Europe, of widespread development of anoxic–euxinic (sulphide-rich) bottom waters in restricted basins that strongly affected marine ecosystems (Jenkyns, 2003, 2010; Caswell and Coe, 2013; Hermoso et al., 2013; Ullmann et al., 2014; Danise et al., 2015). Globally significant burial of photosynthetically derived (<sup>12</sup>C-rich) organic matter took place, producing a positive (with higher δ<sup>13</sup>C) carbon-isotope excursion (CIE) of ~3‰ in marine carbonate and ~4‰ in bulk sedimentary organic matter, which lasted for ~3.5 Myr, from the latest Pliensbachian (latest *spinatum* Zone) until midway through the Toarcian (*bifrons* Zone, *fibulatum* Subzone) (Jenkyns et al., 2002; Gradstein et al., 2012; Hermoso et al., 2013). This observed early Toarcian positive CIE was interrupted by the characteristic abrupt negative shift (to lower δ<sup>13</sup>C) that occurred synchronously with the T-OAE (early Toarcian *tenuicostatum*–*serpentinum* zones) (Jenkyns and Clayton, 1997; Jenkyns, 2003). The magnitude of the T-OAE negative CIE can be as great as ~7‰ in marine and terrestrial organic carbon-isotope records and ~3–6‰ in pelagic and shallow-water carbonates and compound-specific biomarkers (Küspert, 1982; Jenkyns and Clayton, 1986; Hesselbo et al., 2000, 2007; Sælen et al., 2000; Schouten et al., 2000; Jenkyns et al., 2002; Kemp et al., 2005; Hermoso et al., 2009; Sabatino et al., 2009; Al-Suwaidi et al., 2010, 2016; French et al., 2014; Suan et al., 2015).

The T-OAE was preceded by the Pliensbachian–Toarcian boundary event, with a smaller 2–3‰ negative CIE and significant marine benthic and pelagic extinctions (Little and Benton, 1995; Pálffy and Smith, 2000; Cecca and Machioni, 2004; Hesselbo et al., 2007; Caswell et al., 2009; Littler et al., 2010; Caruthers et al., 2013; Percival et al., 2016; Bodin et al., 2016). This earlier event is suggested to have been similar to the T-OAE, and possibly closely coupled to an early but distinct phase of Karoo–Ferrar LIP volcanism, as illustrated by elevated sedimentary mercury (Hg) concentrations and osmium-isotope ratios (<sup>187</sup>Os/<sup>188</sup>Os) that suggest an increase in continental weathering (Percival et al., 2015, 2016).

Although the T-OAE negative CIE is clearly expressed in many different marine and continental basins from both hemispheres (Jenkyns et al., 2001, 2002; Hesselbo et al., 2000, 2007; Kemp et al., 2005; Hermoso et al., 2009; Al-Suwaidi et al., 2010, 2016; Fu et al., 2016; Them et al., 2017; Xu et al., 2017), the interplay between global and local processes varies between depositional environments. Despite the overwhelming evidence for significant global change during the T-OAE, subsequent environmental evolution is largely unconstrained, in part due to a lack of study of biostrati-

graphically complete sedimentary archives that span the complete Toarcian Stage.

Here, we present sedimentological, geochemical and biological data, spanning the nearly complete Toarcian Stage, from the Llanbedr (Mochras Farm) Borehole (hereafter referred to as Mochras), Cardigan Bay Basin, Wales, UK. The Mochras core records a ~260 m thick essentially biostratigraphically complete Toarcian succession that formed in a hemipelagic, open-marine setting facing the proto-North Atlantic Ocean (O’Sullivan et al., 1971). Our study provides a high-resolution geochemical reference record and offers an understanding of the global vs local controls on palaeoenvironmental and palaeoceanographic changes in the relatively open-marine Cardigan Bay Basin.

## 2. Geological setting and stratigraphy

The thick, biostratigraphically well-defined Mochras core covers some 27 Myr of Early Jurassic Earth history from the Hettangian to Toarcian (Woodland, 1971; Gradstein et al., 2012; Hesselbo et al., 2013). In the Early Jurassic, the Cardigan Bay Basin was located at a mid-palaeo-latitude, at the southern end of the European epicontinental seaway that linked the north-western Tethys Ocean to the Boreal Sea (Fig. 1; Sellwood and Jenkyns, 1975; Torsvik et al., 2012).

The Cardigan Bay Basin fill was downthrown against the Early Paleozoic Welsh Massif by a major normal fault system, comprising the Bala, Mochras and Tonfanau faults at the eastern and south-eastern margins of the basin in Late Paleozoic–Early Mesozoic time (Woodland, 1971; Tappin et al., 1994). The Mochras Borehole was drilled onshore by the British Geological Survey (BGS) and Aberystwyth University, between 1967 and 1969, on the Cardigan Bay coast, at Llanbedr, Gwynnedd, northwest Wales (Woodland, 1971; Dobson and Whittington, 1987; Hesselbo et al., 2013; Copestake and Johnson, 2014). The core extends down to the continental Triassic, and Paleogene–Neogene sandstones together with Quaternary glaciogenic sediments overlie the Jurassic section unconformably. The Lower Jurassic succession in this onshore borehole has a thickness of ~1300 m (1906.78–601.83 m below surface (mbs)), much thicker than coeval onshore sections in other parts of the UK and continental Europe (Dobson and Whittington, 1987; Ruhl et al., 2016).

The eight ammonite zones and five foraminiferal zones of the Toarcian Stage in NW Europe have all been recognised in the Mochras core (Ivimey-Cook, 1971; Page, 2003; Simms et al., 2004; Copestake and Johnson, 2014). The ammonite zones and subzones are referred to as zones and subzones hereafter, and are named by a typifying species (e.g. *tenuicostatum* Zone). In addition, belemnites, bivalves, brachiopods, and calcareous nannofossils occur regularly throughout the core, and crinoid ossicles are locally common, but only up to the top Pliensbachian (no crinoid ossicles occur in the Toarcian). Macroscopic plant debris commonly occurs throughout the Pliensbachian and Toarcian succession, and within the Toarcian it is especially enriched in the lower Toarcian interval, coeval with levels rich in siliciclastic silt and sand at around 809–826 m depth, suggesting relatively close proximity to nearby landmasses (Cope, 1984). The dominant, moderately homogeneous lithology of dark grey mudstone and marl beds, alternating with pale grey muddy limestone beds, was deposited in a relatively open-marine sedimentary environment (Sellwood and Jenkyns, 1975).

Specifically, in the lower Toarcian part of the Mochras core, from 831 to 800 m depth, covering the *exaratum* Subzone of the *serpentinum* (= *falciferum*) Zone, sediments are characterised by carbonate-poor mudstone with centimetre-thick laminated dark grey-brown shale at some levels. The *exaratum* Subzone also exhibits several intervals with coarser grained (silty) beds, com-

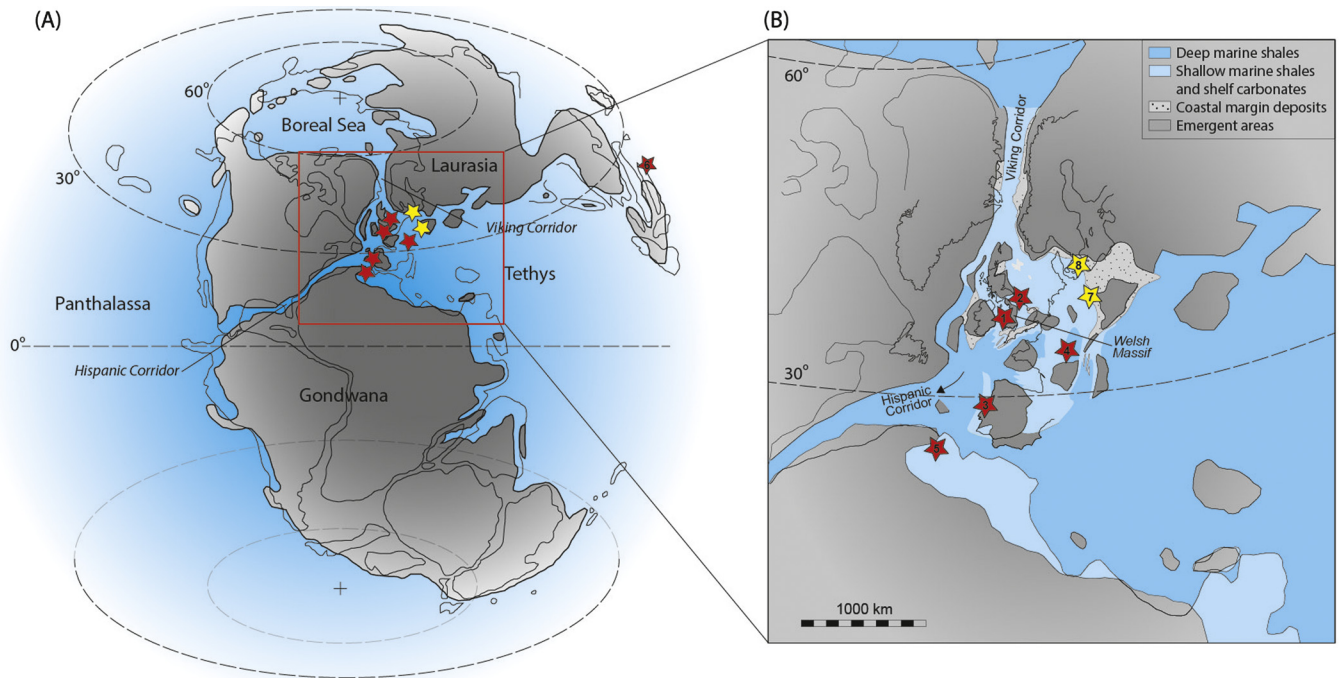


**Fig. 1.** Palaeogeography and location maps. (A) Early Jurassic global palaeogeography, modified from Dera et al. (2011b) and Korte et al. (2015). (B) A more detailed map of the area within the sub-central square in map A, illustrates the palaeogeographic locations of (1) Mochras (Wales), (2) Yorkshire (England), (3) Peniche (Portugal), (4) Beaujolais (France) and (5) Dades (Morocco), marked by a red star, representing marginal to deeper marine depositional environments. The palaeogeographic locations of (7) Kozłowice (Poland) and (8) Bornholm (Denmark), marked by a yellow star, represent coastal to shallow-marginal marine depositional environments. Sakuraguchi (Japan) (6) is marked on the northeast margin of map A. (For interpretation of the colours in this figure, the reader is referred to the web version of this article.)

monly with macroscopic (mm-wide) wood fragments, as well as sedimentary structures such as current ripples and horizons of soft-sediment deformation. Bioturbation is present throughout the Toarcian except for the sporadic intervals of laminated dark grey-brown shale. Siderite nodules regularly occur throughout the *tenuicostatum* and *serpentinum* zones, and are especially pronounced from 852.58 to 819.90 m depth (O'Sullivan et al., 1971; Woodland, 1971). The overlying *bifrons*, *variabilis*, and lower *thouarsense* zones are generally richer in carbonate and record pronounced alternations of marly limestone/carbonate-rich mudstone and carbonate-poor mudstone, at metre-scale. These alternations are similar to those observed in the Pliensbachian strata of the same core (Ruhl et al., 2016).

### 3. Materials and methods

The Mochras slabbed core and registered specimens are housed in the collections of the British Geological Survey, Keyworth, Nottingham, UK. The Toarcian Stage in the Mochras borehole occurs over the depths of 863.50 to 601.83 m. The core slabs of the Toarcian are reasonably well preserved (~96% are present in the archive half of the section), especially in comparison with the Hettangian and Sinemurian intervals, for which material is only patchily available (Hesselbo et al., 2013; Ruhl et al., 2016). A total of 923 samples were collected. Materials for geochemical and sedimentological studies were taken from the slabbed core of the entire Toarcian succession, with a ~33 cm resolution from 863.5 to 843.3 mbs and 809.6 to 601.83 mbs, and at ~25 cm intervals between 843.3 and 809.6 mbs (Supplementary Materials, Table 1). Further samples were collected at levels marked by specific sedimentary features. The fragmented condition of the core in parts of the *tenuicostatum* Zone and the *exaratum* Subzone of the *serpentinum* Zone may have added a few centimetres of uncertainty on the stratigraphic position of individual samples. Potential strati-

graphic uncertainties are therefore negligible relative to the sample resolution and the extremely expanded nature of the section.

Detailed information on laboratory procedures for bulk (total) organic carbon-isotope ( $\delta^{13}\text{C}_{\text{TOC}}$ ) analyses (427 samples), Rock-Eval pyrolysis (248 samples), molecular biomarker analyses (7 samples), Scanning Electron Microscopy (SEM) (21 samples), X-ray diffraction (XRD) (70 samples), Inductively Coupled Plasma Mass Spectrometry (ICP-MS) (19 samples) and hand-held X-ray fluorescence (HH-XRF) (648 samples) is given in the Supplementary Materials.

## 4. Results and discussion

### 4.1. High-resolution chemostratigraphic reference record for the Toarcian Stage

Earlier chemostratigraphic studies on the Toarcian in the Mochras core showed the characteristic overarching positive excursion interrupted by a negative CIE in  $\delta^{13}\text{C}_{\text{TOC}}$  and  $\delta^{13}\text{C}_{\text{carb}}$  (bulk carbonate) records for the T-OAE (Jenkyns and Clayton, 1997; Jenkyns et al., 2001, 2002; Jenkyns, 2003; Katz et al., 2005; van de Schootbrugge et al., 2005), as well as a negative CIE in  $\delta^{13}\text{C}_{\text{TOC}}$  and  $\delta^{13}\text{C}_{\text{carb}}$  at the Pliensbachian–Toarcian boundary (van de Schootbrugge et al., 2005; Percival et al., 2016). The new high-resolution  $\delta^{13}\text{C}_{\text{TOC}}$  record presented here for the uppermost Pliensbachian and entire Toarcian Stage in the Mochras core shows a ~4‰ overall positive carbon-isotope excursion, spanning the uppermost *spinatum* to mid-*bifrons* (*fibulatum* Subzone) zones (Fig. 2). A stratigraphically short-lived ~2‰ negative CIE at the Pliensbachian–Toarcian boundary occurs close to the base of, and is superimposed onto, the observed overall early Toarcian positive CIE (Fig. 2). The maximum of the early Toarcian positive carbon-isotope excursion is interrupted by the stratigraphically extended early Toarcian negative CIE of ~7‰ (–24 to –31‰), which is marked by a step-wise onset at the *tenuicostatum*–*serpentinum* Zone transition (Fig. 2). The Mochras  $\delta^{13}\text{C}_{\text{TOC}}$

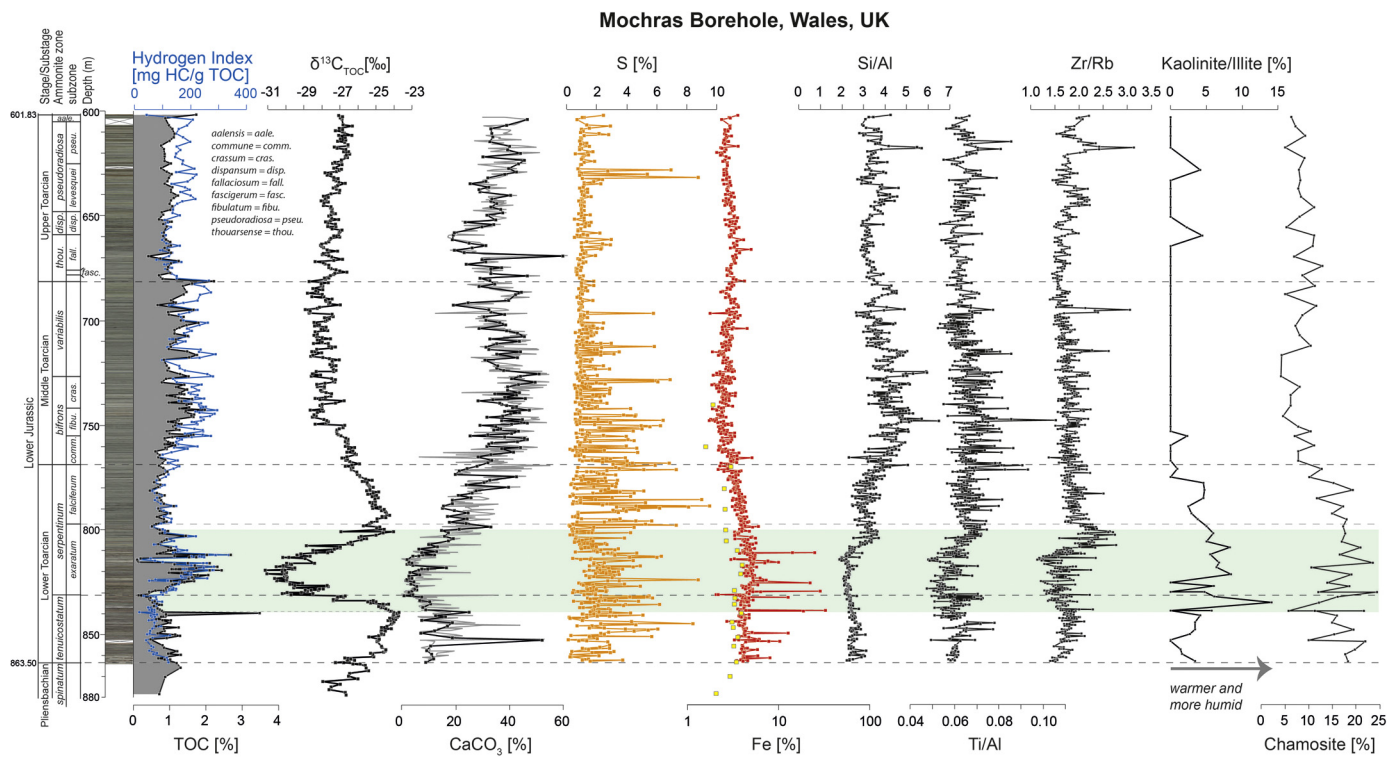


**Fig. 2.** High-resolution geochemical data for the entire Toarcian succession in the Mochras core. TOC and HI measured by Rock Eval are in black and dark blue square symbols, respectively. TOC data of the *spinatum* Zone are from Percival et al. (2015).  $\delta^{13}\text{C}_{\text{TOC}}$  data around the Pliensbachian–Toarcian boundary are from Percival et al. (2016). Concentrations of Fe (red squares), sulphur (yellow squares), ratios of Si/Al, Ti/Al and Zr/Rb (black squares) were measured by HH-XRF; Fe concentrations (yellow squares) were also measured by ICP-MS. The percentage  $\text{CaCO}_3$  (black squares) was reconstructed from Rock-Eval-analysed mineral carbon concentrations (assuming all mineral carbon occurs as  $\text{CaCO}_3$ ); the percentage  $\text{CaCO}_3$  (grey lines) was also reconstructed from Ca concentrations measured by HH-XRF (assuming that all Ca occurs as  $\text{CaCO}_3$ ); ratios of kaolinite/illite and chamosite concentrations were measured by XRD analyses. (For interpretation of the colours in this figure, the reader is referred to the web version of this article.)

record is further characterised by metre-scale  $\sim 1\%$   $\delta^{13}\text{C}_{\text{TOC}}$  fluctuations superimposed on the long-term trend throughout the Toarcian (Fig. 2). The negative steps in  $\delta^{13}\text{C}$  at the onset of the T-OAE negative CIE have been previously observed in both organic and inorganic matter in the Mochras core and in other marine successions (Figs. 2 and 3; Jenkyns et al., 2001, 2002; Kemp et al., 2005; Hesselbo et al., 2007; Hermoso et al., 2009; Sabatino et al., 2009; Them et al., 2017). The T-OAE negative CIE interval in the Mochras core is represented by mudstone and marly limestone, with a TOC content of up to 2.5% and the occurrence of sub-centimetre-thick laminated black shale at some levels (Figs. 2, 3 and 5C; Jenkyns and Clayton, 1997). Through the rest of the Toarcian Stage at Mochras, the TOC values fluctuate between 0.5–1.5%, with on average slightly higher values in the *bifrons* and *variabilis* zones (Fig. 2), and the sediment is generally represented by dark/light grey mudstone.

Hydrogen Index (HI) values are elevated up to 339 mg HC/g TOC in the early Toarcian negative CIE interval, compared to pre-excursion values of less than 100 mg HC/g TOC, and post-excursion values of  $\sim 100$  mg HC/g TOC, but with also elevated values of up to 296 mg HC/g TOC in the *bifrons* and *variabilis* zones (Fig. 2). Increased HI values in the T-OAE negative CIE interval suggest a change in organic-matter type, possibly resulting from elevated marine (algal) primary productivity and supply of organic carbon into the sedimentary environment (Figs. 2 and 3), and/or enhanced preservation of marine organic matter due to water-column stratification. This supposition is supported by the biomarker  $\text{C}_{30}$  24-*n*-propyl sterane, commonly sourced from marine chrysophyte algae, that was detected in the total lipid extracts.  $\text{C}_{30}$ -Sterane indices ( $\text{C}_{30}/(\text{C}_{27} + \text{C}_{28} + \text{C}_{29} + \text{C}_{30})$ ), reflecting the marine vs terrigenous organic-matter input (Moldowan et al.,

1985), are between 0.014 and 0.041, with relatively elevated values in the levels of the T-OAE negative CIE, coinciding with relatively elevated HI values (Fig. 3).  $\text{C}_{30}$ - $\beta\beta$ -Hopanes are also present in the branched-cyclic fractions of the lipid extracts, suggesting an immature to early mature burial history for the sedimentary organic matter in the Mochras core (Seifert and Moldowan, 1980), which is further supported by Toarcian  $T_{\text{max}}$  values of 413–441 °C.

The stratigraphic correlation between the Mochras core and its coeval strata from Yorkshire, UK, based on ammonite biostratigraphy, shows negative CIEs of similar magnitude in both sections, at the Pliensbachian–Toarcian boundary and the T-OAE interval (Fig. 4; Cohen et al., 2004; Kemp et al., 2005; Littler et al., 2010). Actual  $\delta^{13}\text{C}_{\text{TOC}}$  values of the T-OAE negative CIE are, however, different, with  $\delta^{13}\text{C}_{\text{TOC}}$  ranging from  $-24\%$  to  $-31\%$  in the Mochras record, whilst values range from  $-25\%$  to  $-33\%$  in the coeval Yorkshire section (Fig. 4). The observed offset in absolute values between the two successions may be caused by the different compositions of the bulk organic matter. In the Mochras core, terrestrial material accounts for a higher percentage of the total organic matter, as suggested by the abundant macrofossil wood, and HI values only extending up to 339 mg HC/g TOC (Figs. 2 and 3). However, in the Yorkshire coast successions, the bulk sedimentary organic matter likely contains a higher percentage of algal-sourced organic matter, as suggested by HI values of up to 734 mg HC/g TOC (Sælen et al., 2000; French et al., 2014). During the Early Jurassic, marine algae generally also took up a higher proportion of the light ( $^{12}\text{C}$ ) carbon compared to terrestrial higher plants, especially in their ligno-cellulose components, resulting in lower  $\delta^{13}\text{C}_{\text{TOC}}$  values in terrestrial organic matter (van Bergen and Poole, 2002).

Following the broad, overall, positive CIE spanning the uppermost *spinatum* to mid-*bifrons* zones in the Mochras core, the

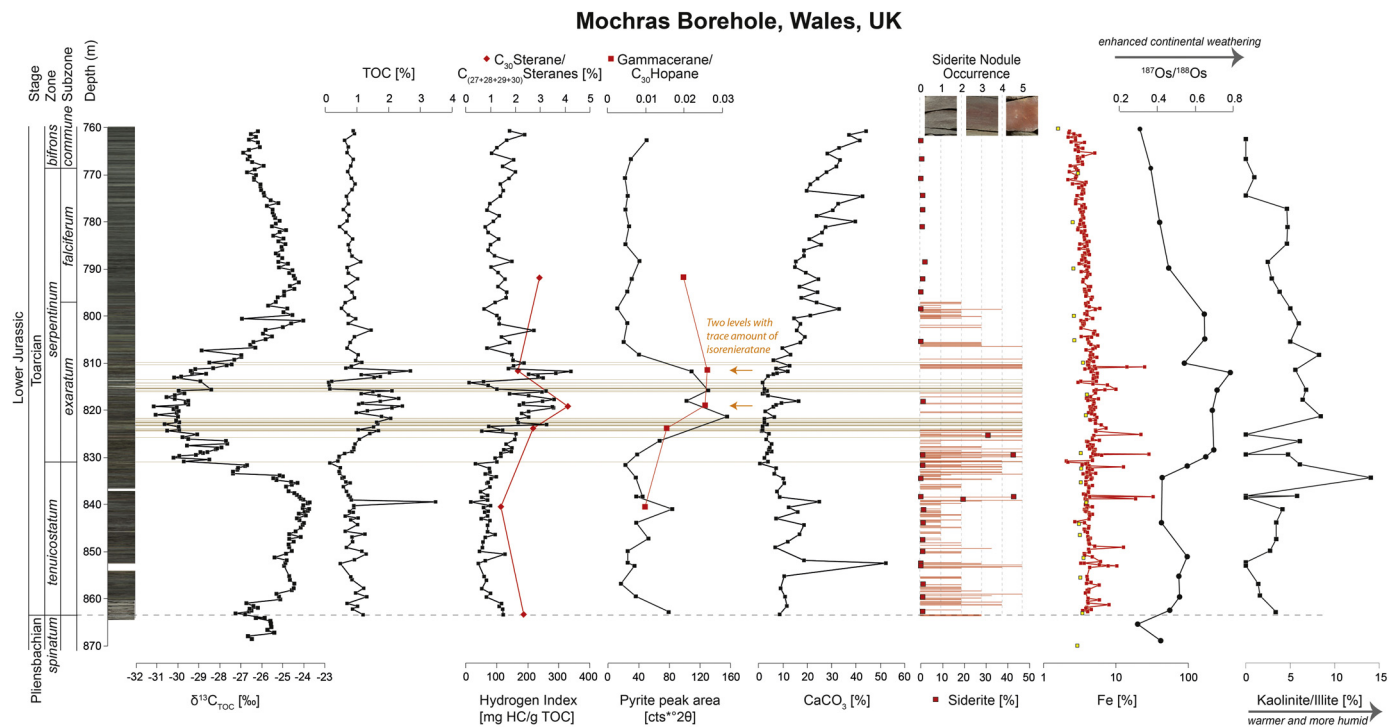


**Fig. 3.** Lithological log and various geochemical records from the lower Toarcian succession of the Mochras core. The occurrences of fine-scale (cm-thick) gravity-flow deposits in the Mochras core is represented by brown horizontal lines.  $\delta^{13}\text{C}_{\text{TOC}}$ , TOC, HI,  $\% \text{CaCO}_3$  and kaolinite/illite ratios are plotted in black squares.  $\text{C}_{30}$  Sterane indices are plotted in red diamonds in the same column as the HI data. The relative changes in pyrite concentration are shown as the variations in peak area of the XRD spectra (black squares). The gammacerane biomarker index is shown using red squares. The occurrence of siderite nodules is based on the visual estimation of the degree of red colouring on the core-slab: colour intensity is shown by red lines on a scale of 0 to 5. The percentage of siderite in some samples was also measured by XRD (red squares in the same column). Fe concentrations measured by HH-XRF and ICP-MS are plotted on a logarithmic scale, in red and yellow squares, respectively.  $^{187}\text{Os}/^{188}\text{Os}$  ratios (full black circles) are from Percival et al. (2016). (For interpretation of the colours in this figure, the reader is referred to the web version of this article.)

$\delta^{13}\text{C}_{\text{TOC}}$  composition of sedimentary organic matter shifted to lower values in the upper *bifrons* and *variabilis* zones, where TOC contents generally increased up to 2.2% and HI values up to 296 mg HC/g TOC. Stratigraphically higher in the section, in the upper Toarcian *thouarsense*–*aalensis* zones,  $\delta^{13}\text{C}_{\text{TOC}}$  increases to be  $\sim 1\text{‰}$  more positive and the TOC and HI values drop down again to  $\sim 1\%$  and  $\sim 100$  mg HC/g TOC, respectively (Fig. 2).

In contrast to many coeval marine basins that were subject to significant burial of organic matter during the T-OAE, the Cardigan Bay Basin is marked by a relative lack of distinct black shale beds. However, because of the widespread synchronous burial of organic carbon in continental and marine basins elsewhere, the broad positive excursion in global  $\delta^{13}\text{C}$ , interrupted by the Pliensbachian–Toarcian and early Toarcian negative excursions recording input of isotopically light carbon, is clearly recorded in the Mochras core, thereby also indicating a relatively continuous sedimentary record.

#### 4.2. Depositional environment and palaeoenvironmental change in the Cardigan Bay Basin

Toarcian bottom waters in the Cardigan Bay Basin at Mochras were generally oxygenated, as indicated by the common and sustained bioturbation throughout most of the succession. The abundance of gammacerane in the lower Toarcian strata at Mochras is very low, even in the darker mudstone beds (with thin discrete layers of laminated black shale; Fig. 3 and 5C) of the *tenuicostatum* and *serpentinum* zones. Gammacerane is a biomarker derived from tetrahymanol that forms in abundance under conditions of high bacterial productivity within stratified water columns, often in lakes or isolated marine basins (Sinninghe Damsté et al., 1995). Hence, the generally low abundance of this biomarker suggests a lack of strong or persistent stratification in the water column. Notably, however, trace amounts of the biomarker isorenieratane

were detected at two horizons, where gammacerane indices are also slightly elevated, within the part of the T-OAE negative CIE with the lowest  $\delta^{13}\text{C}_{\text{TOC}}$  values, at  $\sim 811.66$  m and  $\sim 819.10$  m in the *exaratum* Subzone (Fig. 3). Isorenieratane is a pigment of photosynthetic green sulphur bacteria *Chlorobiaceae*, which photosynthesize utilising hydrogen sulphide ( $\text{H}_2\text{S}$ ) and sunlight (Koopmans et al., 1996). Hence, the presence of isorenieratane or its diagenetic and catagenetic products in sedimentary rocks or crude oils is an indication for photic-zone euxinia in the water column (Koopmans et al., 1996). The two horizons where isorenieratane was detected, albeit in trace amounts, are darker in colour and laminated, with no bioturbation at the scale of visual description, suggesting anoxic to euxinic conditions in the photic zone and at the seafloor (Fig. 5C). These levels also have higher TOC values of up to 2.7% and elevated HI, suggesting elevated planktonic productivity and/or preservation as a possible primary control on the relatively high content of organic matter.

Faunal evidence also suggests that geochemical and physical conditions (e.g. oxygen, temperature, pH) in the water column of the Cardigan Bay Basin may, at times, however, have been less than favourable for marine organisms. Belemnites occur commonly in the upper Pliensbachian *spinatum* Zone at Mochras, but they become rare in the darker mudstone of the lowermost Toarcian *tenuicostatum* Zone and the lower half of the *serpentinum* Zone (*exaratum* Subzone) (Fig. 4). Cumulative belemnite counts on the slabbed core surface of the upper Pliensbachian and Toarcian succession (Fig. 4) show a gap in belemnite occurrence stratigraphically overlapping with observed belemnite gaps in other lower Toarcian marine successions in north-western and southern Europe (Fig. 4; Hesselbo et al., 2007; Ullmann et al., 2014). The stratigraphic disappearance of these molluscs is hence in accord with organic geochemical data from the Mochras core that imply environmental deterioration. Belemnite abundance in the Cleve-



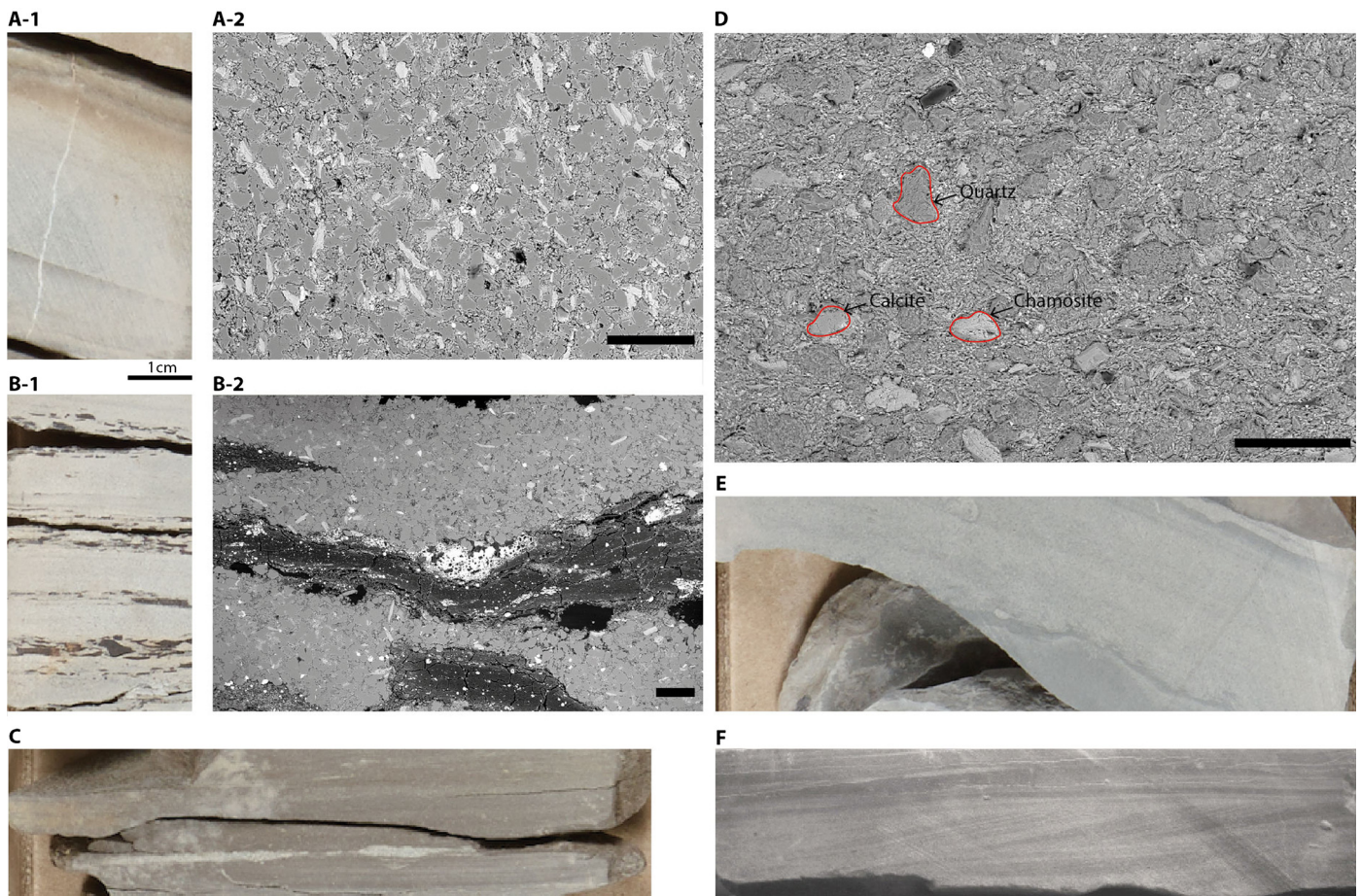


**Fig. 5.** Core photographs (A-1, B-1, C, E and F with a 1 cm scale bar) and BSEM images (A-2, B-2 and D; the black scale bars in the SEM images represent 200  $\mu\text{m}$ ) of gravity-flow deposits from the Toarcian of the Mochras core. Image A-1: the upper brown interval illustrates a turbidite; the accompanying BSEM image A-2 indicates that this layer is predominantly composed of fine silt-grade quartz grains. Images B-1 and B-2 illustrate another turbidite, which exhibits abundant macroscopic wood fragments; the BSEM image (B-2) shows woody material (black) surrounded by detrital quartz grains of fine-silt size. Image (C) illustrates a centimetre-scale fine-grained dark mudstone with faint lamination (depth 819.10 m). Image (D) is from a common type of mudstone horizon (842.04 m), and illustrates silt-grade detrital grains of quartz, calcite and chamosite. Image (E) shows a flame structure at depth 814.20 m. Image (F) illustrates a ripple at depth 814.78 m.

*exaratum* Subzone), may have made low–mid palaeolatitude (shallow) marine basins, including the relatively open-marine Cardigan Bay Basin, temporarily unfavourable for micro- and macroscopic fauna to thrive, and/or be preserved.

Concentrations of calcium carbonate ( $\text{CaCO}_3$ ) are very low in the lower Toarcian of the Mochras core, especially in the *exaratum* Subzone of the *serpentinum* Zone, where  $\delta^{13}\text{C}_{\text{TOC}}$  values are most negative (Fig. 2). Values increase to up to 50% in the stratigraphically higher *bifrons* and *variabilis* zones (Fig. 2). The observed distinct minimum in  $\text{CaCO}_3$  concentrations during the T-OAE negative CIE may have resulted from strongly reduced primary productivity of marine calcifiers, perhaps with concomitant increase of organic-walled plankton and bacteria (Jenkyns, 1988; Mattioli et al., 2009). Such a phenomenon was possibly linked to near-surface acidification due to the increase of  $p\text{CO}_2$  in the ocean–atmosphere system (McElwain et al., 2005; Hönisch et al., 2012), and a rise of the carbonate compensation depth (CCD) into shallow shelf basins (Jenkyns, 2010). Increased riverine input may have further diluted  $\text{CaCO}_3$  concentrations through addition of fine-grained siliciclastic sediment (Fig. 3).

Kaolinite content in the Toarcian at Mochras varies between 0 and ~5%, and illite (all polymorphs including those of the mica family) content range between 18% and 36%. Kaolinite at Mochras cannot be clearly imaged using back-scattered SEM (BSEM) or analysed by energy-dispersive X-ray spectroscopy (EDS), possibly because of the tiny size of the detrital mineral particles of this soil-

borne mineral, which is typically less than 2  $\mu\text{m}$  (cf. Hesselbo et al., 2009). Authigenic kaolinite generally has a larger particle size (Chamley, 1979), and is not observed in the 21 samples studied by SEM. An initial chemical weathering mechanism for kaolinite release is also suggested by broad XRD peak-profiles, confirming the small particle size and/or poor crystallinity. The formation of kaolinite in soils is generally favoured under warm and humid climatic conditions, promoted by elevated hydrological cycling, increased rainfall and groundwater-flow through weathering profiles. Such processes favour leaching of metal cations and reduction of soil pH, both factors that together favour the formation of kaolinite over smectite (Millot, 1970; Thiry, 2000).

XRD analysis indicates that the (illite-rich) illite-smectite in the studied samples has a small proportion of swelling layers (<20%), which is characteristic of detrital clay weathered and re-worked from mature rocks and deposited as fine-grained sediments (Moore and Reynolds, 1997). The composition of the detrital clay mineral assemblages may therefore reflect the prevalent climatic conditions in the hinterland. Hence detrital kaolinite/illite (K/I) ratios may be used as a proxy for the reconstruction of relative temperature and humidity changes, as in the Upper Jurassic Kimmeridge Clay Formation (Hesselbo et al., 2009) and across the Paleocene–Eocene boundary off Antarctica (Robert and Kennett, 1994). In the Mochras core, K/I ratios are distinctly elevated through the T-OAE negative CIE, with a return to nearly zero for the remainder of the Toarcian (Fig. 2). This pat-

tern is consistent with intensified hydrological cycling and globally increased silicate weathering. It is exemplified by elevated  $^{187}\text{Os}/^{188}\text{Os}$  values during the T-OAE in the Mochras core, under warm and more humid climatic conditions in the hinterland surrounding the open-marine Cardigan Bay Basin, due to elevated atmospheric  $p\text{CO}_2$  and associated global warming (Jenkyns, 2003; Cohen et al., 2004; McElwain et al., 2005; Dera et al., 2011a; Kemp et al., 2011; Brazier et al., 2015; Percival et al., 2016). Relatively elevated kaolinite abundances in lower Toarcian strata are also observed (at least) regionally, in many marine sections in northern and central Europe (e.g. France, Hungary, Poland, Portugal, Switzerland), suggesting a more widespread change to warmer and more humid conditions in the hinterland and increased continental weathering (Deconinck and Bernoulli, 1991; Duarte, 1998; Raucsik and Varga, 2008; Dera et al., 2009; Brański, 2010; Hermoso and Pellenard, 2014).

#### 4.3. Silt-sized sediment supply and continental weathering during the T-OAE

A fluctuating, non-biogenic sediment supply to the Cardigan Bay Basin during the early Toarcian OAE is possibly indicative of changing climatic and environmental conditions on nearby landmasses and in shallow marine environments. Changes in siliciclastic sediment supply and mineral grain size through the Toarcian in the Mochras core are indicated by changes in elemental ratios calculated from measurements by HH-XRF. In sedimentary rocks, elemental non-biogenic silicon (Si) is commonly sourced either from relatively coarser grained quartz or from finer grained aluminosilicates, whereas aluminium (Al) is generally sourced only from aluminosilicates (Calvert and Pedersen, 2007). No biogenic silica has been observed using the SEM, suggesting that this material is either not present or exists only in trace quantities. The Al-normalised Si concentration in the studied rocks therefore likely reflects changes in the amount of quartz relative to aluminosilicate phases in the sediments. Titanium (Ti) also resides in aluminosilicates as a substituent for other major elements, as well as in discrete Ti-oxide and silicate mineral phases, commonly as rutile inclusions in quartz. Sedimentary zirconium (Zr) occurs almost exclusively in the mineral zircon ( $\text{ZrSiO}_4$ ), especially in fine sand and silt fractions. Rubidium (Rb) substitutes readily for potassium (K) in aluminosilicate minerals. Ti/Al and Zr/Rb ratios may therefore represent a proxy for grain size, since quartz and associated minerals are the main contribution for coarser grains (Calvert and Pedersen, 2007).

In the Mochras core, the sedimentary Si/Al, Ti/Al and Zr/Rb ratios overall decrease in parallel upwards, from the onset of the T-OAE negative CIE to the middle of the *exaratum* Subzone (Fig. 2; Supplementary Fig. 1), followed by increasing values during the subsequent recovery of  $\delta^{13}\text{C}_{\text{TOC}}$  to higher values (Fig. 2). This pattern suggests a greater proportion of fine-grained siliciclastic (clay) accumulation relative to silt in the basin over the interval of the early Toarcian negative CIE, possibly in response to coeval eustatic sea level rise and the associated palaeocoastline retreat away from the study location (Figs. 2 and 8). Furthermore, enhanced early Toarcian hydrological cycling may have increased chemical and physical weathering of soils and bedrock in the hinterland, increasing the supply of fine-grained sediments, such as clays, to nearby marine basins, which is also supported by the observed increased kaolinite/illite ratios in parallel with elevated  $^{187}\text{Os}/^{188}\text{Os}$  values during the T-OAE in the Mochras core (Figs. 2 and 6). The T-OAE negative CIE interval is, however, also the only stratigraphic interval in the entire Lower Jurassic succession in the Mochras core that is characterised by discrete thin beds of pale-coloured, quartzose siltstone within the mudstone, some of which are faintly laminated or rippled, or include cm-scale woody fragments (Fig. 5

A-1, A-2, B-1, B-2, F). These 1–10 cm thick siltstone beds appear in two ~3-m-thick stratigraphic intervals in the *exaratum* Subzone (lower *serpentinum* Zone), at around 815 and 823 m depth, and their occurrence is superimposed on the overall decrease in siliciclastic grain size at that time (Fig. 3). Individual siltstone beds probably formed from gravity flows originating from the nearby basin margins (potentially the closely adjacent Mochras Fault footwall), and thus suggest enhanced supply of clastic sediments and relatively rapid transportation in turbulent flows. Unlike the low gradient sediment dispersal systems that would have characterised the regional muddy sediment supply, sediments shed directly off an adjacent steep footwall would have been insensitive to sea-level changes, a setting similar to that supposed for the Peniche section within the palaeo-Lusitanian Basin (Hesselbo et al., 2007).

The Ti/Al and Zr/Rb elemental ratios relatively stabilise following the T-OAE negative CIE; however, metre-scale fluctuations continue to occur in concordance with the limestone-marl lithological couplets throughout the middle and upper Toarcian part of the Mochras core (Fig. 2). Si/Al ratios also continue to rise to more positive values in the *bifrons* Zone, where Ti/Al ratios are more variable (Fig. 2).

XRD analyses of sediments throughout the Toarcian in the Mochras core show the presence of calcite, chamosite, illite and mica, illite-rich illite-smectite, quartz, a minor amount of (and in places near-absent) Fe-dolomite, kaolinite, K-feldspar, plagioclase, siderite and pyrite (see also the Supplementary Materials section). Silt-sized calcite, chamosite, mica, and quartz, which are of detrital origin, were also observed by SEM-EDS analyses (Fig. 5-D). The silt-sized detrital minerals were possibly sourced from the Paleozoic rocks of nearby landmasses, such as the Welsh Massif, but the provenance of the different sediment components at Mochras remains unconfirmed at present (Figs. 1 and 8).

The occurrence of coarser grained deposits during the most negative interval of the T-OAE negative CIE in the Mochras core coincides stratigraphically with similar lithologies in other shallower and deeper marine basins, from different palaeolatitudes in different parts of the world. These areas include the Sakuraguchi-Dani section in the Tabe Basin (Japan), Beaujolais (France), the Lusitanian Basin (Portugal), and the High Atlas Basin (Morocco) (Fig. 1 and 6; Hesselbo et al., 2007; Suan et al., 2013; Kemp and Izumi, 2014; Pittet et al., 2014; Krencker et al., 2015; Izumi et al., 2018). In detail, at Sakuraguchi-Dani, Japan, sandstone beds occur in a silty mudstone interval where the degree of bioturbation (measured by ichnofabric index) is higher, whereas in the dark mudstone interval where the degree of bioturbation is lower, no sandstone beds were observed (Kemp and Izumi, 2014). Similarly, at Peniche, Portugal the percentage of insoluble residue (a measure of siliciclastic vs calcareous input) goes up during the T-OAE negative CIE, suggesting an overall higher relative supply of siliciclastic input under fully oxygenated depositional conditions (Hesselbo et al., 2007). The temporally restricted occurrence of coarser-grained sediment supply, in many cases as debris flows/turbidity currents, in geographically widespread marine basins and during the early Toarcian negative CIE and corresponding global change event, suggests a climatic control rather than only local (extensional) tectonic activity. The observation suggests an increased supply of clastic sediments into marginal and deeper marine basins in response to increased runoff and/or storm-driven currents (Hesselbo et al., 2007; Kemp and Izumi, 2014; Krencker et al., 2015). Similar inferences of increased sediment supply were also made for the coastal and marginal marine sections of southwest Bornholm (Denmark) and the Polish Basin (Fig. 1; McElwain et al., 2005; Hesselbo and Pieńkowski, 2011). Local bathymetric conditions, however, likely affected the physical characteristics of sediments, and their fluxes, in the gravity-flows. The mineral grain-size in the gravity-flow deposits in the lower Toarcian strata of Mochras is,



for example, much finer, and the individual beds are much thinner (1–10 cm) than those in the coeval strata of Peniche (Lusitanian Basin, Portugal), likely reflecting the contrasting basement lithology of each basin.

Globally enhanced continental weathering during the T-OAE has been suggested by different geochemical proxies. Strontium-isotope ( $^{87}\text{Sr}/^{86}\text{Sr}$ ) values from early Toarcian seawater, as recorded in belemnite calcite, show an Early Jurassic low of  $\sim 0.70707$  (normalised to a value of 0.710248 for NIST 987) at around the Pliensbachian–Toarcian transition (Jones et al., 1994; McArthur et al., 2000). Values increased slightly (from  $\sim 0.70707$  to  $\sim 0.70710$ ) over the lower Toarcian *tenuicostatum* Zone (Fig. 6). This shift is suggestive of a changing balance towards the supply of radiogenic strontium from the global weathering of continental crustal materials to the global oceans, and/or relative decreasing supply of unradiogenic strontium from the weathering of island arcs and hydrothermal circulation through mid-ocean ridges (Palmer and Edmond, 1989, 1992; Allègre et al., 2010). The subsequent accelerated increase in  $^{87}\text{Sr}/^{86}\text{Sr}$  to values of  $\sim 0.70716$  in the *exaratum* Subzone (lower *serpentinum* Zone) (Fig. 6), suggests an accelerated change in this balance that likely represents an enhanced radiogenic strontium flux to the global oceans. This flux is possibly the fingerprint of strongly enhanced early Toarcian hydrological cycling and increased weathering of continental crust. The early Toarcian seawater  $^{187}\text{Os}/^{188}\text{Os}$  record, analysed from Yorkshire and Mochras (Figs. 3 and 6), shows an initial increase at the Pliensbachian–Toarcian boundary followed by a stronger and more prolonged shift during the T-OAE negative CIE (Cohen et al., 2004; Percival et al., 2016). This pattern is also interpreted to reflect directly the supply of more radiogenic Os isotopes to the global oceans due to elevated continental weathering (Cohen et al., 2004; Percival et al., 2016). The observed T-OAE negative excursion in seawater calcium-isotope ratios ( $\delta^{44}/^{40}\text{Ca}$ ), recorded at Peniche, Portugal from brachiopod calcite and bulk rock (Fig. 6; Brazier et al., 2015) is similarly interpreted as due to a climatically controlled increase in the rate of continental weathering, as well as a drop in the carbonate accumulation rate due to ocean acidification.

The stratigraphic correspondence between changes in early Toarcian seawater  $^{87}\text{Sr}/^{86}\text{Sr}$ ,  $^{187}\text{Os}/^{188}\text{Os}$ ,  $\delta^{44}/^{40}\text{Ca}$  and the temporally restricted and geographically widespread occurrence of coarser grained gravity-flow deposits in shallow- and deeper marine basins during the T-OAE is strongly suggestive of a common forcing mechanism. Although the expression of the different proxies might have been affected by differences in global elemental residence time and/or local overprints, the changes suggest enhanced hydrological cycling in response to greenhouse-gas-induced climatic warming during the T-OAE that accelerated continental weathering, and caused increased supply of sediment to continental margins and intra-marginal marine basins. These data also suggest that the highest rate of hydrological cycling occurred coevally, at different palaeolatitudes, when the carbon-isotope composition of the global ocean-atmosphere system was at its most negative, with the rate of  $^{12}\text{C}$ -enriched  $\text{CO}_2/\text{CH}_4$  release outcompeting the rate of  $^{12}\text{C}$ -enriched organic-carbon burial in oceans and lakes.

#### 4.4. Early Toarcian siderite formation in the Cardigan Bay Basin and its potential relevance for the early Toarcian global sulphur cycle

Pink to red coloured nodules, with varying concentrations of iron minerals, are common in the Mochras core from the Pliensbachian–Toarcian boundary to the uppermost level of the T-OAE negative CIE (from 863.6–796.8 m depth; *tenuicostatum* Zone–*exaratum* Subzone; Fig. 3). Although the original colour of freshly cut surfaces of these nodules is brown, oxidation of iron minerals in the nodules likely resulted in the red colour of the slabbed and exterior surfaces of the core (Fig. 7) that occurred over the sev-

eral decades since the core was drilled and slabbed. XRD analyses of four of the red nodular horizons that are rich in ferrous minerals show that siderite makes up 22%–47% of the total mineral content (Fig. 3). These red beds were avoided for  $\delta^{13}\text{C}_{\text{TOC}}$  analyses (Supplementary Materials).

The morphology of the siderite minerals and the diagenetic pathways along which they may have formed were studied with BSEM and EDS (Fig. 7). In the siderite nodules, relicts of high-magnesium (Mg) calcite crystals (identified by EDS analysis) partially replaced and overgrown by siderite, occur in the lower Toarcian of the Mochras core, suggesting that the high-Mg calcite may have acted as a nucleus for siderite growth (Fig. 7-g). Some of the observed holes in the centre of the siderite crystals may originally have been high-Mg calcite nuclei that were subsequently dissolved (Fig. 7-h; cf. Huggett et al., 2000). Siderite, however, not only occurs in distinct nodules, but also in the matrix of the more silty gravity-flow sedimentary structures described above. Centimetre-scale ripple cross-lamination with reddish-grey coloured, siderite-rich fine-sediment drapes occur, for example, at, but not limited to,  $\sim 815.59$  mbs in the Mochras core (Fig. 7-a). Siderite within these ripples of fine sand is exclusively concentrated in the finer-grained laminae (Fig. 7-e), possibly due to more reducing pore fluids in the lower permeability environment of the finer grained intervals.

Siderite generally forms as an early diagenetic mineral in a low-sulphate, reducing environment with abundant iron and  $\text{CO}_3^{2-}$  availability (e.g. Curtis and Spears, 1968; Huggett et al., 2000, and references therein). However, pyrite framboids (diameter  $> 10 \mu\text{m}$ ), whose formation requires reduced sulphur, are also observed, especially within bioclasts that are enclosed by siderite-rich sediments or nodules (Fig. 7-f). Pyrite framboids of this diameter probably formed first during early diagenesis in response to the oxidation of organic matter within these bioclasts, with the concomitant reduction of  $\text{Fe}^{3+}$  and sulphate (Wilkin et al., 1996). Subsequent depletion of sulphate in the pore waters likely resulted in the further availability of  $\text{Fe}^{2+}$  that, together with the  $\text{CO}_3^{2-}$  in the pore waters, may have initiated the formation of siderite.

Elevated pyrite concentrations (reflected by pyrite XRD peak areas) in the lower Toarcian of Mochras (Fig. 2) are stratigraphically coincident with increased TOC values across the T-OAE negative CIE (Fig. 3). Sulphur concentrations are also broadly elevated in the lower Toarcian interval (Fig. 2). Elevated sulphur and pyrite concentrations in the sediments have been observed in other marine T-OAE successions (e.g. Wignall et al., 2010; Kemp et al., 2011), suggesting major sulphur drawdown from the global ocean reservoir by the massive burial of pyrite across the European epicontinental seaway, on continental margins and in the open ocean basins of the Tethys and elsewhere. This process resulted in a major perturbation of the global sulphur cycle as registered by an increase in the sulphur-isotope composition ( $\delta^{34}\text{S}$ ) of global seawater, as manifested in carbonate associated sulphur-isotope records ( $\delta^{34}\text{S}_{\text{CAS}}$ ), which initiated at, or close to, the Pliensbachian–Toarcian transition and co-occurred with the overall early Toarcian positive CIE (Fig. 9; Gill et al., 2011; Newton et al., 2011). The estimated rate and magnitude of change in the global sulphur cycle suggests significantly lower sulphate concentrations globally (Newton et al., 2011) that could have facilitated early diagenetic siderite generation in sulphate-poor pore waters of the Cardigan Bay Basin. This suggested strong reduction in global ocean sulphate concentrations as a result of large-scale pyrite burial is likely to have taken place against a background of reduced-salinity marine waters already pre-conditioned by widespread Early Jurassic evaporite deposition during the onset of rifting between North America and Europe/North Africa (Austin et al., 1989; Davison, 2005) and along the south-western passive margin of the Tethys Ocean (Chandler et al., 1992).

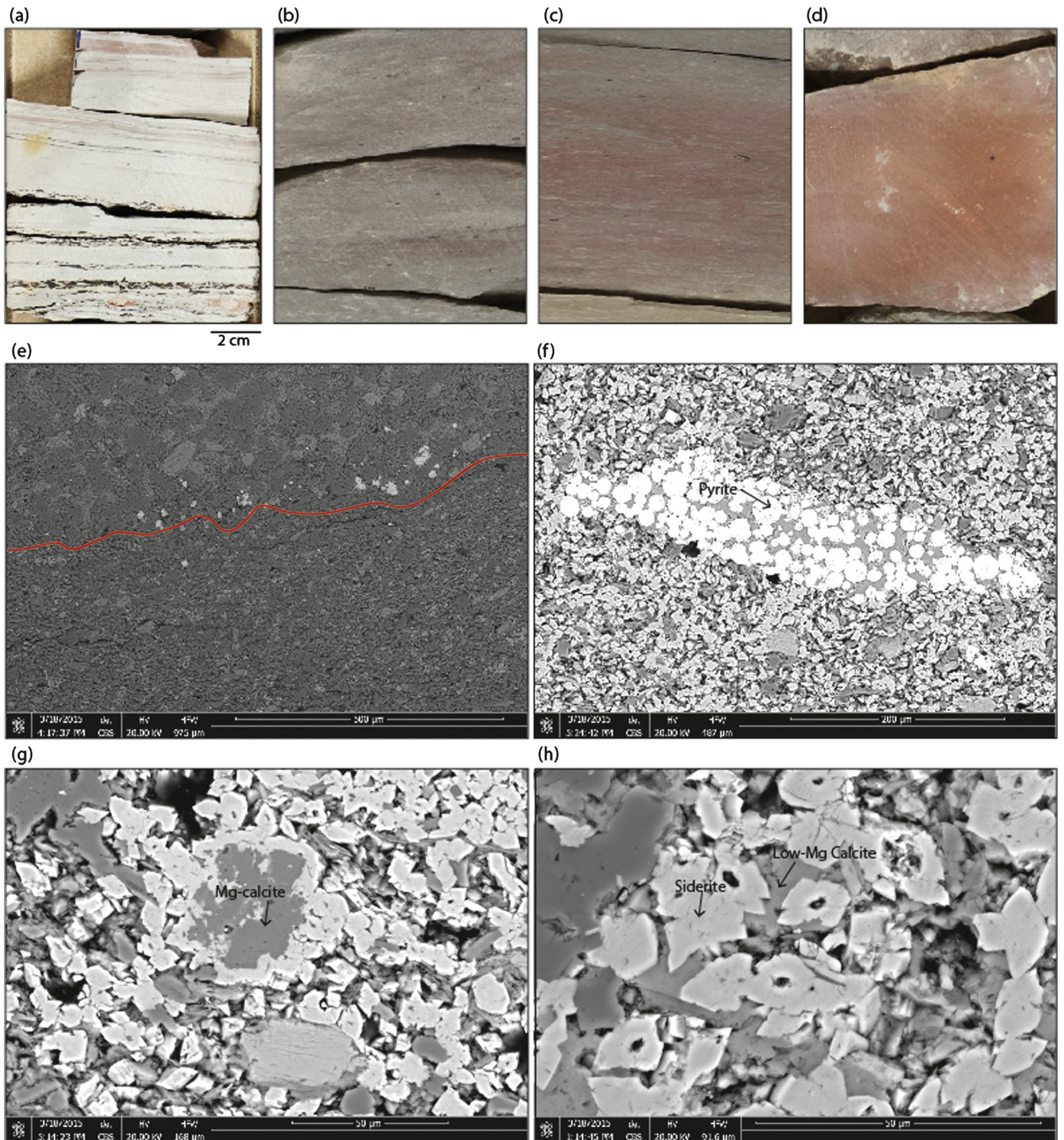
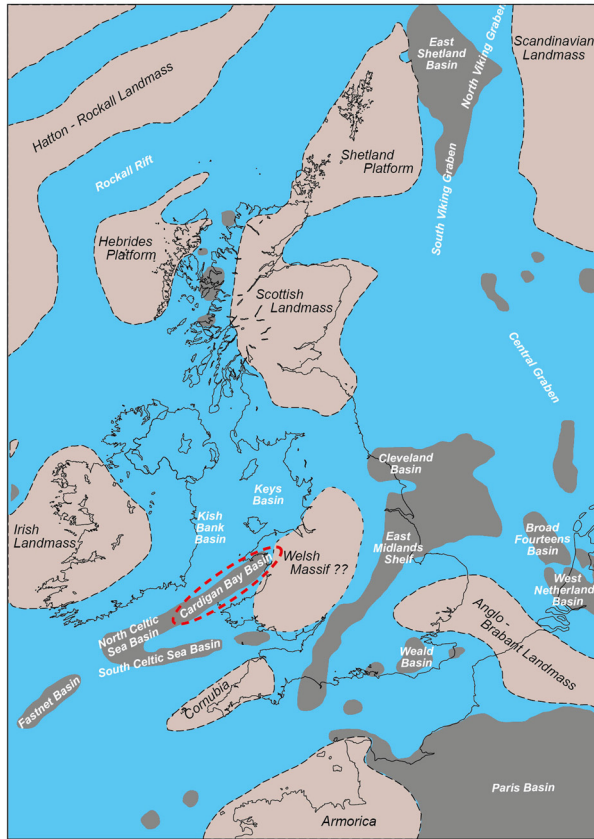


**Fig. 7.** Photographs of slabbed core (a–d) and SEM photomicrographs (e–h) of selected siderite-bearing beds from the Toarcian of the Mochras core. The 2 cm scale bar applies to all four images. Image (a) from 815.59 m in the Mochras core contains cm-scale ripple-drift cross-lamination with thin red-coloured layers due to the presence of oxidised siderite (upper part of the image) and turbidites with wood fragments (lower part of the image). Images (b), (c) and (d) illustrate varying degrees of red colouration on the core slab, by oxidation of siderite. Image (e): back-scattered scanning electron microscopy (BSEM) image of the sedimentary horizon in image (a); the red line marks the boundary between finer grained sediments below and coarser grained sediments above. The pale minerals in the finer grained area (lower half of the image) are siderite. By contrast, in the upper, coarser grained region, no siderite is present. Image (f): pyrite framboids have (partly) replaced the bioclast and siderite occurs throughout the matrix. Image (g): high-Mg calcite (medium grey) is enclosed by siderite (pale grey). Image (h): siderite crystals marked by hollow cores, which were originally probably filled by high-Mg calcite; the surrounding matrix comprises low-Mg calcite cement. (For interpretation of the references to colour in this figure, the reader is referred to the web version of this article.)

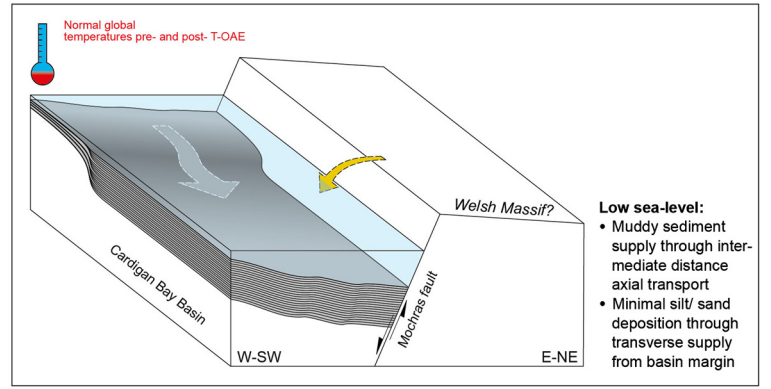
Iron (Fe) elemental concentrations in the Toarcian of Mochras, measured by hand-held XRF and ICP-MS, show elevated concentrations of up to 6% in the non-siderite-bearing beds of the T-OAE

negative CIE interval, significantly higher than the average values of ~2% in the non-siderite-bearing beds underlying and overlying the T-OAE negative CIE interval (Figs. 2 and 3). There are also dis-

Early Jurassic (middle Toarcian) palaeogeography



Pre- & post- T-OAE negative CIE



T-OAE negative CIE

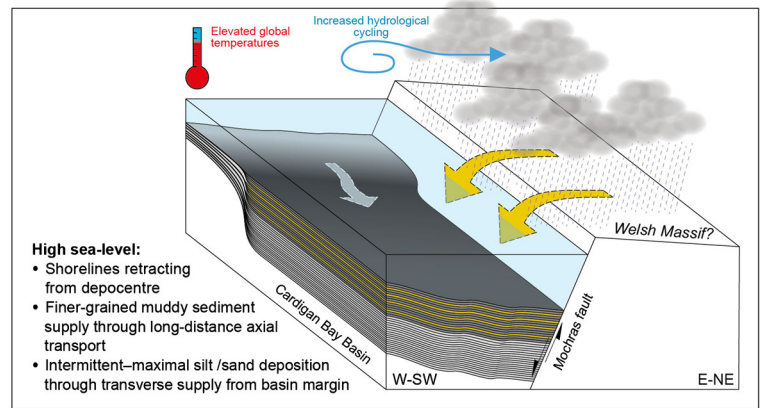


**Fig. 8.** Map of the regional palaeogeography of the early-middle Toarcian northwest European epicontinental seaway and the early Toarcian depositional model for the Cardigan Bay Basin (Cope et al., 1992). The pre- and post- early Toarcian negative CIE muddy sediments were supplied axially into the Cardigan Bay Basin. During the early Toarcian negative CIE and the associated eustatic sea level rise finer grained clay sediments were supplied from retracting shorelines bordering nearby landmasses. These landmasses were also subject to increased physical and chemical weathering in response to elevated atmospheric  $pCO_2$  and the associated increased hydrological cycling, which partly led to intermittent supply of coarser grained silty to sandy gravity flows into the Cardigan Bay Basin during the early Toarcian negative CIE.

Mochras Borehole, Cardigan Bay Basin, UK

Monte Sorigenza, Italy

Yorkshire, Cleveland Basin, UK

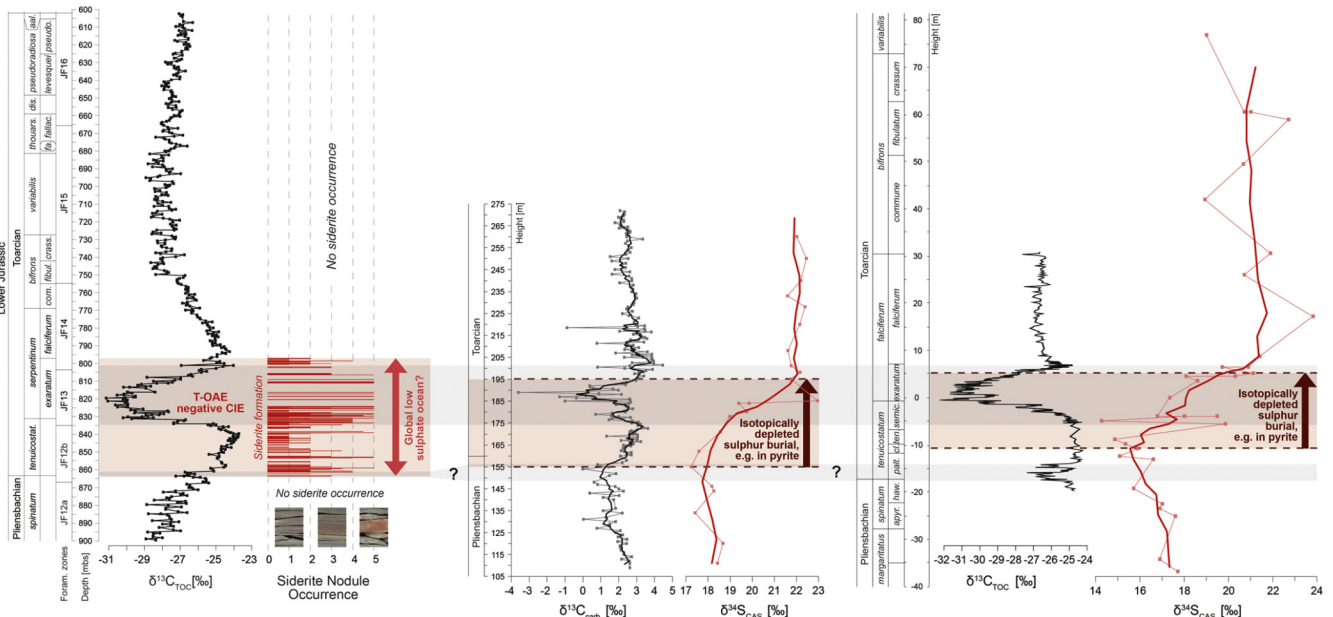


**Fig. 9.** Stratigraphic correlation between siderite formation in the Cardigan Bay Basin and a strong increase in global seawater  $\delta^{34}S$ , as manifested in  $\delta^{34}S_{CAS}$  records, and based on carbon-isotope and ammonite biostratigraphy. The carbon-isotope record and siderite bed occurrences in the Mochras core are from this study. The carbon-isotope and the carbonate associated sulphur-isotope records are from Monte Sorigenza (Italy; Woodfine et al., 2008; Gill et al., 2011) and the Yorkshire coast (Cleveland Basin, UK; Cohen et al., 2004; Kemp et al., 2005; Littler et al., 2010; Gill et al., 2011). The carbon-isotope ratios are marked as grey dots and black lines. The sulphur-isotope ratios and their five point averages are marked as red squares and red lines, respectively. (For interpretation of the references to colour in this figure, the reader is referred to the web version of this article.)

crete highs of ~33% Fe in the observed siderite nodules (Fig. 3). In the Mochras core, Fe in non-siderite-bearing beds largely exists in chamosite minerals (Fe-rich chlorite). Based on SEM study, the chamosite minerals are largely detrital (Fig. 5–D). The elevated chamosite contents in the T-OAE interval probably reflects enhanced detrital iron-rich clay mineral supply from the hinterland. This suggests either intensified continental weathering, possibly under higher atmospheric CO<sub>2</sub> concentrations and/or enhanced hydrological cycling or, alternatively, a shift in provenance. A detrital origin of some chamosite from physical weathering of the Lower Paleozoic metamorphic rocks of surrounding landmasses, such as the Welsh Massif or even the Scottish and Irish Landmasses (Fig. 8), is most likely. Alternatively, but likely with a minor contribution, high weathering intensity would also result in the supply of sufficient iron (e.g. from soils), which could favour chamosite formation in the remains of organisms or in faecal pellets close to the sediment–water interface, as found today seaward of large tropical deltas (Porrenga, 1965, 1967).

Siderite formation has been observed in many ancient and modern marine successions. The upper Pliensbachian Cleveland Ironstone of Yorkshire, which is mainly composed of siderite and chamosite, is thought to have precipitated during intervals of low sedimentation rates to ensure sufficient iron supply into the pore waters, but with a diminished supply of sulphate (Curtis and Spears, 1968; Sellwood, 1971). Siderite cements in the Eocene of Whitecliff Bay (Isle of Wight, UK) occur with different associated facies and formed in a weakly oxidising depositional environment, also with low sedimentation rates and during an interval directly preceding stratigraphic break or hiatus (Huggett et al., 2000). Siderite is also formed in the present-day inner shelf muds of the Amazon river, with elevated Fe supply (which leaves plenty of Fe for reduction and to react with carbonate once sulphate is exhausted) through the weathering of soils under humid and tropical hinterland conditions, the low supply and dilution of reactive organic matter (due to the commonly dominant input of usually more refractory terrestrial organic matter together with high sedimentation rates), and the high physical mobility of sediments, which promotes oxidative recharge (Aller et al., 1986). The inferred sedimentation rate in the early Toarcian Cardigan Bay Basin was 2–3 times higher than in coeval successions from the Cleveland and Lusitanian basins. The combined stratigraphic thickness of the *tenuicostatum* and *serpentinum* zones in Mochras, Peniche and Yorkshire is ~90 m, ~35 m and ~22 m, respectively. The TOC content, with predominantly terrestrial components, is relatively low in the lower Toarcian succession of Mochras. The supply of reactive Fe was, however, relatively elevated at the time of deposition. Geochemical conditions favourable to siderite formation in the pore waters of the lower Toarcian of the Cardigan Bay Basin may therefore in some major aspects resemble conditions in the present-day sediments of the Amazon shelf, albeit with a depositional environment that might have been much deeper.

The overall degree of red colouration, reflecting the concentration of siderite minerals, is intensified at the Pliensbachian–Toarcian boundary and during the T-OAE negative CIE (the uppermost-*tenuicostatum* Zone to *exaratum* Subzone), and covaries with <sup>187</sup>Os/<sup>188</sup>Os values (Fig. 3). Globally enhanced weathering rates and the increased local supply of Fe, as suggested by the elevated chamosite concentrations at this stratigraphical interval (Fig. 2), together with a reduced sulphate content in the pore water possibly facilitated by lower global ocean sulphate concentrations, and favourable redox conditions and sedimentation rates, are hypothesised to have been instrumental in the formation of siderite nodules during the early Toarcian in the Cardigan Bay Basin.

## 5. Conclusions

The first high-resolution chemostratigraphic reference record for the near complete Toarcian Stage, from the Llanbedr (Mochras Farm) Borehole, shows a major ~7‰ negative excursion in δ<sup>13</sup>C<sub>TOC</sub>, associated with the T-OAE and superimposed on a broader early Toarcian positive excursion. In contrast to several other epicontinental European seaway marine successions of early Toarcian age, the T-OAE interval in the *exaratum* Subzone of the *serpentinum* Zone of the Mochras core is marked by only transient deposition of black shale beds. The TOC values through the T-OAE at Mochras are, however, relatively elevated, up to ~2.5%, in comparison with the underlying and overlying sediments. Enhanced marine primary productivity and flux of marine algal material to the seafloor during the T-OAE, are indicated by increased HI values of up to ~300 mg HC/g TOC and elevated C<sub>30</sub> sterane indices, possibly in response to relatively elevated nutrient supply and/or increased preservation. Relatively high pyrite concentrations in the interval of the T-OAE negative CIE, together with limited presence of the biomarkers gammacerane and isorenieratane, suggest transient photic-zone euxinia and episodic anoxia at the seafloor. Increased marine organic productivity and preservation likely led to the relatively enriched organic-matter content in the Cardigan Bay Basin during the T-OAE.

Although belemnites occur regularly throughout the Pliensbachian and Toarcian of the Mochras core, their presence is severely diminished in the lower Toarcian interval, from the Pliensbachian–Toarcian boundary to the top of the T-OAE negative CIE. This temporary disappearance in core material is coeval with a lack of these fossils elsewhere in northwest Europe, interpreted as due to regionally extensive anoxic to euxinic bottom waters.

Centimetre-thick silt to fine-sand gravity-flow deposits, and abundant macroscopic wood fragments, occur in two stratigraphic intervals in the *exaratum* Subzone, where the δ<sup>13</sup>C values are most negative. These clastic sediments occur coevally with similar deposits in geographically widespread early Toarcian shallow to deeper marine basins at low to mid-palaeolatitudes. The input of clastic sediments was broadly synchronous with changes in early Toarcian seawater δ<sup>44/40</sup>Ca, <sup>187</sup>Os/<sup>188</sup>Os and <sup>87</sup>Sr/<sup>86</sup>Sr. These observations suggest accelerated continental weathering as the cause of intensified turbidity-current activity, probably in response to enhanced hydrological cycling from greenhouse-gas-induced climatic warming and increased clastic sediment supply and sediment loading in marginal areas. Such a switch to warmer and more humid climatic conditions is further supported by elevated soil-formed-kaolinite to illite ratios in the lower Toarcian of the Mochras core. At the same time, background mudstone beds become finer grained through the T-OAE, an observation possibly partly explained by transgression accompanying the well-documented eustatic sea-level rise at the time, which would likely have pushed back regional sediment-distribution systems leading to overall more distal conditions in basinal settings.

Nodular siderite beds occur from the Pliensbachian–Toarcian boundary up to the top of the T-OAE negative CIE in the Mochras core. Diagenetic siderite minerals in the relatively open-marine hemipelagic Cardigan Bay Basin possibly formed in response to an elevated Fe supply from continental weathering and relatively low sulphate concentrations in global seawater (already pre-conditioned by large-scale evaporite deposition) and pore waters due to large-scale pyrite fixation in globally extensive organic-rich strata (black shales) that are the hallmark of the T-OAE.

## Acknowledgements

We acknowledge funding from Shell International Exploration & Production B.V., the International Continental Scientific Drilling

Program (ICDP), the Natural Environment Research Council (NERC) (grant number NE/N018508/1), and the British Geological Survey. Clemens V. Ullmann acknowledges funding from Leopoldina, Germany National Academy of Sciences (grant number LPDS 2014-08). All authors thank the British Geological Survey (BGS), especially Scott Renshaw and Tracey Gallagher for enabling access to the Mochras core, and Steve Wyatt, Alice Barroll, Jonathan Wells and Phil Holdship (Oxford University) and Chris Kendrick (BGS) for laboratory assistance. Daniel Minisini thanks G. Gil for broadening the horizons. James B. Riding and Melanie J. Leng publish with the approval of the Executive Director of the British Geological Survey (NERC). This manuscript is a contribution to IGCP 655 (IUGS-UNESCO): *Toarcian Oceanic Anoxic Event: Impact on marine carbon cycle and ecosystems*, and IGCP 632 (IUGS-UNESCO): *Continental Crises of the Jurassic: Major Extinction events and Environmental Changes within Lacustrine Ecosystems*.

## Appendix A. Supplementary material

Supplementary material related to this article can be found online at <https://doi.org/10.1016/j.epsl.2017.12.037>.

## References

- Al-Suwaidi, A.H., Angelozzi, G.N., Baudin, F., Damborenea, S.E., Hesselbo, S.P., Jenkyns, H.C., Mancenido, M.O., Riccardi, A.C., 2010. First record of the early Toarcian oceanic anoxic event from the southern hemisphere, Neuquén Basin, Argentina. *J. Geol. Soc. Lond.* 167, 633–636.
- Al-Suwaidi, A.H., Hesselbo, S.P., Damborenea, S.E., Manceñido, M.O., Jenkyns, H.C., Riccardi, A.C., Angelozzi, G.N., Baudin, F., 2016. The Toarcian oceanic anoxic event (Early Jurassic) in the Neuquén Basin, Argentina: a reassessment of age and carbon isotope stratigraphy. *J. Geol.* 124, 171–193.
- Allègre, C.J., Louvat, P., Gaillardet, J., Meynadier, L., Rad, S., Capmas, F., 2010. The fundamental role of island arc weathering in the oceanic Sr isotope budget. *Earth Planet. Sci. Lett.* 292, 51–56.
- Aller, R.C., Mackin, J.E., Cox Jr, R.T., 1986. Diagenesis of Fe and S in Amazon inner shelf muds: apparent dominance of Fe reduction and implications for the genesis of ironstones. *Cont. Shelf Res.* 6, 263–289.
- Austin, J.A., Tucholke, B.E., Uchupi, E., 1989. Upper Triassic–Lower Jurassic salt basin southeast of the Grand Banks. *Earth Planet. Sci. Lett.* 92, 357–370.
- Bailey, T.R., Rosenthal, Y., McArthur, J.M., van de Schootbrugge, B., Thirlwall, M.F., 2003. Paleocceanographic changes of the Late Pliensbachian–Early Toarcian interval: a possible link to the genesis of an Oceanic Anoxic Event. *Earth Planet. Sci. Lett.* 212, 307–320.
- Bodin, S., Krencker, F.-N., Kothe, T., Hoffmann, R., Mattioli, E., Heimhofer, U., Kabiri, L., 2016. Perturbation of the carbon cycle during the late Pliensbachian–early Toarcian: new insight from high-resolution carbon isotope records in Morocco. *J. Afr. Earth Sci.* 116, 89–104.
- Brański, P., 2010. Kaolinite peaks in early Toarcian profiles from the Polish Basin – an inferred record of global warming. *Geol. Q.* 54, 15–24.
- Brazier, J., Suan, G., Tacail, T., Simon, L., Martin, J.E., Mattioli, E., Balter, V., 2015. Calcium isotope evidence for dramatic increase of continental weathering during the Toarcian oceanic anoxic event (Early Jurassic). *Earth Planet. Sci. Lett.* 411, 164–176.
- Burgess, S.D., Bowring, S.A., Fleming, T.H., Elliot, D.H., 2015. High-precision geochronology links the Ferrar large igneous province with early Jurassic ocean anoxia and biotic crisis. *Earth Planet. Sci. Lett.* 415, 90–99.
- Calvert, S.E., Pedersen, T.F., 2007. Elemental proxies for palaeoclimatic and palaeoceanographic variability in marine sediments: interpretation and application. In: Hillaire, C., de Vernal, A. (Eds.), *Proxies in Late Cenozoic Paleocceanography*, vol. 1, Developments in Quaternary Research. Elsevier Science, Amsterdam, pp. 567–644.
- Caruthers, A.H., Smith, P.L., Gröcke, D.R., 2013. The Pliensbachian–Toarcian (Early Jurassic) extinction, a global multi-phased event. *Palaeogeogr. Palaeoclimatol. Palaeoecol.* 386, 104–118.
- Caswell, B.A., Coe, A.L., Cohen, A.S., 2009. New range data for marine invertebrate species across the early Toarcian (Early Jurassic) mass extinction. *J. Geol. Soc. Lond.* 166, 859–872.
- Caswell, B.A., Coe, A.L., 2013. Primary productivity controls on opportunistic bivalves during Early Jurassic oceanic deoxygenation. *Geology* 41, 1163–1166.
- Cecca, F., Macchioni, F., 2004. The two Early Toarcian (Early Jurassic) extinction events in ammonoids. *Lethaia* 37, 35–56.
- Chamley, H., 1979. North-Atlantic clay sedimentation and paleoenvironment since the Late Jurassic. In: Talwani, M., Hay, W., Ryan, W.B.F. (Eds.), *Deep Drilling Results in the Atlantic Ocean: Continental Margins and Paleoenvironments*. In: Maurice Ewing Series, vol. 3. Amer. Geophys. Union, pp. 342–361.
- Chandler, M.A., Rind, D., Ruedy, R., 1992. Pangaeon climate during the Early Jurassic: GCM simulations and the sedimentary record of paleoclimate. *Geol. Soc. Am. Bull.* 104, 543–559.
- Cohen, A.S., Coe, A.L., Harding, S.M., Schwark, L., 2004. Osmium isotope evidence for the regulation of atmospheric CO<sub>2</sub> by continental weathering. *Geology* 32, 157–160.
- Cope, J.C.W., 1984. The Mesozoic history of Wales. *Proc. Geol. Assoc.* 95, 373–385.
- Cope, J.C.W., Ingham, J.K., Rawson, P.F. (Eds.), 1992. *Atlas of Palaeogeography and Lithofacies*. Geological Society, London. Memoir, 13.
- Copestake, P., Johnson, B., 2014. Lower Jurassic Foraminifera from the Llanbedr (Mochras Farm) Borehole, North Wales, UK. *Monograph of the Palaeontographical Society*, vol. 167. 403 p.
- Curtis, C.D., Spears, D.A., 1968. The formation of sedimentary iron minerals. *Econ. Geol.* 63, 257–270.
- Danise, S., Twitchett, R.J., Little, C.T.S., 2015. Environmental controls on Jurassic marine ecosystems during global warming. *Geology* 43, 263–266.
- Davison, I., 2005. Central Atlantic margin basins of North West Africa: geology and hydrocarbon potential (Morocco to Guinea). *J. Afr. Earth Sci.* 43, 254–274.
- Deconinck, J.-F., Bernoulli, L.D., 1991. Clay mineral assemblages of Mesozoic pelagic and flysch sediments of the Lombardian Basin (Southern Alps): implications for palaeotectonics, palaeoclimate and diagenesis. *Geol. Rundsch.* 80 (1), 1–17.
- Dera, G., Pellenard, P., Neige, P., Deconinck, J.-F., Pucéat, E., Dommergues, J.-L., 2009. Distribution of clay minerals in Early Jurassic Peritethyan seas: palaeoclimatic significance inferred from multiproxy comparisons. *Palaeogeogr. Palaeoclimatol. Palaeoecol.* 271, 39–51.
- Dera, G., Brigaud, B., Monna, F., Laffont, R., Pucéat, E., Deconinck, J.-F., Pellenard, P., Joachimski, M.M., Durllet, C., 2011a. Climatic ups and downs in a disturbed Jurassic world. *Geology* 39, 215–218.
- Dera, G., Neige, P., Dommergues, J.-L., Brayard, A., 2011b. Ammonite paleobiogeography during the Pliensbachian–Toarcian crisis (Early Jurassic) reflecting paleoclimate, eustasy, and extinctions. *Glob. Planet. Change* 78, 92–105.
- Dobson, M.R., Whittington, R.J., 1987. The geology of Cardigan Bay. *Proc. Geol. Assoc.* 98, 331–353.
- Duarte, L.V., 1998. Clay minerals and geochemical evolution in the Toarcian–lower Aalenian of the Lusitanian Basin (Portugal). *Cuadernos de Geología Ibérica* 24, 69–98.
- Duncan, R.A., Hooper, P.R., Rehacek, J., Marsh, J.S., Duncan, A.R., 1997. The timing and duration of the Karoo igneous event, southern Gondwana. *J. Geophys. Res.* 102, 18127–18138.
- French, K.L., Sepúlveda, J., Trabuco-Alexandre, J., Gröcke, D.R., Summons, R.E., 2014. Organic geochemistry of the early Toarcian oceanic anoxic event in Hawsker Bottoms, Yorkshire, England. *Earth Planet. Sci. Lett.* 390, 116–127.
- Fu, X., Wang, J., Feng, X., Wang, D., Chen, W., Song, C., Zeng, S., 2016. Early Jurassic carbon-isotope excursion in the Qiangtang Basin (Tibet), the eastern Tethys: implications for the Toarcian Oceanic Anoxic event. *Chem. Geol.* 442, 62–72.
- Gill, C.B., Lyons, T.W., Jenkyns, H.C., 2011. A global perturbation to the sulfur cycle during the Toarcian Oceanic Anoxic Event. *Earth Planet. Sci. Lett.* 312, 484–496.
- Gradstein, F.M., Ogg, J.G., Schmitz, M.D., Ogg, G.M. (Eds.), 2012. *The Geologic Time Scale 2012*. Elsevier B.V., 1176 p.
- Hermoso, M., Callonnet, L.L., Minoletti, F., Renard, M., Hesselbo, S.P., 2009. Expression of the Early Toarcian negative carbon-isotope excursion in separated carbonate microfractions (Jurassic, Paris Basin). *Earth Planet. Sci. Lett.* 277, 194–203.
- Hermoso, M., Minoletti, F., Pellenard, P., 2013. Black shale deposition during Toarcian super-greenhouse driven by sea level. *Clim. Past* 9, 2703–2712.
- Hermoso, M., Pellenard, P., 2014. Continental weathering and climatic changes inferred from clay mineralogy and paired carbon isotopes across the early to middle Toarcian in the Paris Basin. *Palaeogeogr. Palaeoclimatol. Palaeoecol.* 399, 385–393.
- Hesselbo, S.P., Bjerrum, C.J., Hinnov, L.A., MacNiocail, C., Miller, K.G., Riding, J.B., van de Schootbrugge, B., the Mochras Revisited Science Team, 2013. Mochras borehole revisited: a new global standard for Early Jurassic earth history. *Sci. Drill.* 16, 81–91.
- Hesselbo, S.P., Deconinck, J.-F., Huggett, J.M., Morgans-Bell, H.S., 2009. Late Jurassic palaeoclimatic change from clay mineralogy and gamma-ray spectrometry of the Kimmeridge Clay, Dorset, UK. *J. Geol. Soc. Lond.* 166, 1123–1133.
- Hesselbo, S.P., Gröcke, D.R., Jenkyns, H.C., Bjerrum, C.J., Farrimond, P., Bell, H.S.M., Green, O.R., 2000. Massive dissociation of gas hydrate during a Jurassic oceanic anoxic event. *Nature* 406, 392–395.
- Hesselbo, S.P., Jenkyns, H.C., 1995. A comparison of the Hettangian to Bajocian successions of Dorset and Yorkshire. In: Taylor, P.D. (Ed.), *Field Geology of the British Jurassic*. Geological Society, London, pp. 105–150.
- Hesselbo, S.P., Jenkyns, H.C., Duarte, L.V., Oliveira, L.C.V., 2007. Carbon-isotope record of the Early Jurassic (Toarcian) Oceanic Anoxic Event from fossil wood and marine carbonate (Lusitanian Basin, Portugal). *Earth Planet. Sci. Lett.* 253, 455–470.
- Hesselbo, S.P., Pienkowski, G., 2011. Stepwise atmospheric carbon-isotope excursion during the Toarcian Oceanic Anoxic Event (Early Jurassic, Polish Basin). *Earth Planet. Sci. Lett.* 301, 365–372.
- Hönsch, B., Ridgwell, A., Schmidt, D.N., Thomas, E., Gibbs, S.J., Sluijs, A., Zeebe, R., Kump, L., Martindale, R.C., Greene, S.E., Kiessling, W., Ries, J., Zachos, J.C., Royer,

- D.L. Barker, S. Marchitto Jr, T.M., Moyer, R., Pelejero, C., Ziveri, P., Foster, G.L., Williams, B., 2012. The geological record of ocean acidification. *Science* 335, 1058–1063.
- Huggett, J., Dennis, P., Gale, A., 2000. Geochemistry of early siderite cements from the Eocene succession of Whitecliff Bay, Hampshire Basin, UK. *J. Sediment. Res.* 70, 1107–1117.
- Ivimey-Cook, H.C., 1971. Stratigraphical palaeontology of the Lower Jurassic of the Llanbedr (Mochras Farm) Borehole. In: Woodland, A.W. (Ed.), *The Llanbedr (Mochras Farm) Borehole*. Institute of Geological Sciences, pp. 87–92. Report No. 71/18.
- Izumi, K., Kemp, D.B., Itamiya, S., Inui, M., 2018. Sedimentary evidence for enhanced hydrological cycling in response to rapid carbon release during the early Toarcian oceanic anoxic event. *Earth Planet. Sci. Lett.* 481, 162–170.
- Jenkyns, H.C., 1985. The Early Toarcian and Cenomanian–Turonian anoxic events in Europe: comparisons and contrasts. *Geol. Rundsch.* 74, 505–518.
- Jenkyns, H.C., Clayton, C.J., 1986. Black shales and carbon isotopes from the Tethyan Lower Jurassic. *Sedimentology* 33, 87–106.
- Jenkyns, H.C., 1988. The early Toarcian (Jurassic) anoxic event: stratigraphic, sedimentary, and geochemical evidence. *Am. J. Sci.* 288, 101–151.
- Jenkyns, H.C., Clayton, C.J., 1997. Lower Jurassic epicontinental carbonates and mudstones from England and Wales: chemostratigraphic signals and the early Toarcian anoxic event. *Sedimentology* 44, 687–706.
- Jenkyns, H.C., Gröcke, D.R., Hesselbo, S.P., 2001. Nitrogen isotope evidence for water mass denitrification during the early Toarcian (Jurassic) oceanic anoxic event. *Paleoceanography* 16, 593–603.
- Jenkyns, H.C., Jones, C.E., Gröcke, D.R., Hesselbo, S.P., Parkinson, D.N., 2002. Chemostratigraphy of the Jurassic System: applications, limitations and implications for palaeoceanography. *J. Geol. Soc. Lond.* 159, 351–378.
- Jenkyns, H.C., 2003. Evidence for rapid climate change in the Mesozoic–Palaeogene greenhouse world. *Phil. Trans. R. Soc. Lond. A* 361, 1885–1916.
- Jenkyns, H.C., 2010. Geochemistry of oceanic anoxic events. *Geochem. Geophys. Geosyst.* 11, Q03004. <https://doi.org/10.1029/2009GC002788>.
- Jenkyns, H.C., Schouten-Huibers, L., Schouten, S., Sinninghe Damsté, J.S., 2012. Warm Middle Jurassic–Early Cretaceous high-latitude sea-surface temperatures from the Southern Ocean. *Clim. Past* 8, 215–226.
- Jones, C.E., Jenkyns, H.C., Hesselbo, S.P., 1994. Strontium isotopes in Early Jurassic seawater. *Geochim. Cosmochim. Acta* 58, 1285–1301.
- Katz, M.E., Wright, J.D., Miller, K.G., Cramer, B.S., Fennel, K., Falkowski, P.G., 2005. Biological overprint of the geological carbon cycle. *Mar. Geol.* 217, 323–338.
- Kemp, D.B., Coe, A.L., Cohen, A.S., Schwark, L., 2005. Astronomical pacing of methane release in the Early Jurassic period. *Nature* 437, 396–399.
- Kemp, D.B., Coe, A.L., Cohen, A.S., Weedon, G.P., 2011. Astronomical forcing and chronology of the early Toarcian (Early Jurassic) oceanic event in Yorkshire, UK. *Paleoceanography* 26, PA4210. <https://doi.org/10.1029/2011PA002122>.
- Kemp, D.B., Izumi, K., 2014. Multiproxy geochemical analysis of a Panthalassic margin record of the early Toarcian oceanic anoxic event (Toyora area, Japan). *Paleoceanogr. Palaeoclimatol. Palaeoecol.* 414, 332–341.
- Koopmans, M.P., Köster, J., van Kaam-Peters, H.M.E., Kenig, F., Schouten, S., Hartgers, W.A., de Leeuw, J.W., Sinninghe Damsté, J.S., 1996. Diagenetic and catagenetic products of isorenieratane: molecular indicators for photic zone anoxia. *Geochim. Cosmochim. Acta* 60, 4467–4496.
- Korte, C., Hesselbo, S.P., Ullmann, C.V., Dietl, G., Ruhl, M., Schweigert, G., Thibault, N., 2015. Jurassic climate mode governed by ocean gateway. *Nat. Commun.* 6, 10015.
- Krenker, F.-N., Bodin, S., Suan, G., Heimhofer, U., Kabiri, L., Immenhauser, A., 2015. Toarcian extreme warmth led to tropical cyclone intensification. *Earth Planet. Sci. Lett.* 425, 120–130.
- Küspert, W., 1982. Environmental changes during oil shale deposition as deduced from stable isotope ratios. In: Einsele, G., Seilacher, A. (Eds.), *Cyclic and Event Stratification*. Springer, Berlin, pp. 482–501.
- Little, C.T., Benton, M.J., 1995. Early Jurassic mass extinction: a global long-term event. *Geology* 23, 495–498.
- Littler, K., Hesselbo, S.P., Jenkyns, H.C., 2010. A carbon-isotope perturbation at the Pliensbachian–Toarcian boundary: evidence from the Lias Group, NE England. *Geol. Mag.* 147, 181–192.
- Mattioli, E., Pittet, B., Petitpierre, L., Mailliot, S., 2009. Dramatic decrease of pelagic carbonate production by nanoplankton across the Early Toarcian anoxic event (T-OAE). *Glob. Planet. Change* 65, 134–145.
- McArthur, J.M., Donovan, D.T., Thirlwall, M.F., Fouke, B.W., Matthey, D., 2000. Strontium isotope profile of the early Toarcian (Jurassic) oceanic anoxic event, the duration of ammonite biozones, and belemnite palaeotemperatures. *Earth Planet. Sci. Lett.* 179, 269–285.
- McElwain, J.C., Wade-Murphy, J., Hesselbo, S.P., 2005. Changes in carbon dioxide during an oceanic anoxic event linked to intrusion into Gondwana coals. *Nature* 435, 479–482.
- Millot, G., 1970. *Geology of Clays: Weathering, Sedimentology, Geochemistry*. Springer-Verlag/Chapman & Hall, New York/London. 429 p.
- Moldowan, J.M., Seifert, W.K., Gallegos, E.J., 1985. Relationship between petroleum composition and depositional environment of petroleum source rocks. *Am. Assoc. Pet. Geol. Bull.* 69, 1255–1268.
- Moore, D.M., Reynolds, R.C., 1997. *X-Ray Diffraction and the Identification and Analysis of Clay Minerals*, second edition. Oxford University Press, Oxford, New York.
- Mutterlose, J., Malkoč, M., Schouten, S., Sinninghe Damsté, J.S., Forster, A., 2010. TEX<sub>86</sub> and stable  $\delta^{18}\text{O}$  paleothermometry of early Cretaceous sediments: implications for belemnite ecology and paleotemperature proxy application. *Earth Planet. Sci. Lett.* 298, 286–298.
- Newton, R.J., Reeves, E.P., Kafousia, N., Wignall, P.B., Bottrell, S.H., Sha, J.-G., 2011. Low marine sulfate concentrations and the isolation of the European epicontinental sea during the Early Jurassic. *Geology* 39, 7–10.
- O’Sullivan, K.N., Ivimey-Cook, H.C., Lewis, B.J., Harrison, R.K., 1971. Log of the Llanbedr (Mochras Farm) Borehole. In: Woodland, A.W. (Ed.), *The Llanbedr (Mochras Farm) Borehole*. In: Report of the Institute of Geological Sciences, vol. 71/18, pp. 11–35.
- Page, K.N., 2003. The Lower Jurassic of Europe: its subdivision and correlation. *Geol. Surv. Den. Greenl. Bull.* 1, 23–59.
- Pálffy, J., Smith, P.L., 2000. Synchrony between Early Jurassic extinction, oceanic anoxic event, and the Karoo–Ferrar flood basalt volcanism. *Geology* 28, 747–750.
- Palmer, M.R., Edmond, J.M., 1989. The strontium isotope budget of the modern ocean. *Earth Planet. Sci. Lett.* 92, 11–26.
- Palmer, M.R., Edmond, J.M., 1992. Controls over the strontium isotope composition of river water. *Geochim. Cosmochim. Acta* 56, 2099–2111.
- Percival, L.M.E., Witt, M.L.L., Mather, T.A., Hermoso, M., Jenkyns, H.C., Hesselbo, S.P., Al-Suwaidi, A.H., Storm, M.S., Xu, W., Ruhl, M., 2015. Globally enhanced mercury deposition during the end-Pliensbachian and Toarcian OAE: a link to the Karoo–Ferrar Large Igneous Province. *Earth Planet. Sci. Lett.* 428, 267–280.
- Percival, L.M.E., Cohen, A.S., Davies, M.K., Dickson, A.J., Hesselbo, S.P., Jenkyns, H.C., Leng, M.J., Mather, T.A., Storm, M.S., Xu, W., 2016. Osmium isotope evidence for two pulses of increased continental weathering linked to Early Jurassic volcanism and climate change. *Geology* 44, 759–762.
- Pittet, B., Suan, G., Lenoir, F., Duarte, L.V., Mattioli, E., 2014. Carbon isotope evidence for sedimentary discontinuities in the lower Toarcian of the Lusitanian Basin (Portugal): sea level change at the onset of the Oceanic Anoxic Event. *Sediment. Geol.* 303, 1–14.
- Porrenga, D.H., 1965. Chamosite in recent sediments of the Niger and Orinoco Deltas. *Geol. Mijnb.* 44, 400–403.
- Porrenga, D.H., 1967. Glauconite and chamosite as depth indicators in the marine environment. *Mar. Geol.* 5, 495–501.
- Raiswell, R., Canfield, D.E., 2012. The iron biogeochemical cycle past and present. *Geochem. Perspect.* 1 (1), 1–220.
- Raucsik, B., Varga, A., 2008. Climato-environmental controls on clay mineralogy of the Hettangian–Bajocian successions of the Mecsek Mountains, Hungary: An evidence for extreme continental weathering during the early Toarcian oceanic anoxic event. *Paleoceanogr. Palaeoclimatol. Palaeoecol.* 265, 1–13.
- Robert, C., Kennett, J.P., 1994. Antarctic subtropical humid episode at the Paleocene–Eocene boundary: clay-mineral evidence. *Geology* 22, 211–214.
- Ruhl, M., Hesselbo, S.P., Hinnov, L., Jenkyns, H.C., Xu, W., Storm, M.S., Riding, J.B., Minisini, D., Ullmann, C.V., Leng, M.J., 2016. Astronomical constraints on the duration of the Early Jurassic Pliensbachian Stage and global climatic fluctuations. *Earth Planet. Sci. Lett.* 455, 149–165.
- Sabatino, N., Neri, R., Bellanca, A., Jenkyns, H.C., Baudin, F., Parisi, G., Masetti, D., 2009. Carbon-isotope records of the early Jurassic (Toarcian) oceanic anoxic event from the Valdorbica (Umbria–Marche Apennines) and Monte Mangart (Julian Alps) sections: palaeoceanographic and stratigraphic implications. *Sedimentology* 56, 1307–1328.
- Sælen, G., Tyson, R.V., Telnæs, N., Talbot, M.R., 2000. Contrasting watermass conditions during deposition of the Whitby Mudstone (Lower Jurassic) and Kimmeridge Clay (Upper Jurassic) formations, UK. *Paleoceanogr. Palaeoclimatol. Palaeoecol.* 163, 163–196.
- Schouten, S., van Kaam-Peters, H.M.E., Rijpstra, W.I.C., Schoell, M., Sinninghe-Damsté, J.S., 2000. Effects of an Oceanic Anoxic Event on the stable carbon isotopic composition of Early Toarcian carbon. *Am. J. Sci.* 300, 1–22.
- Seifert, W.K., Moldowan, J.M., 1980. The effect of thermal stress on source-rock quality as measured by hopane stereochemistry. *Phys. Chem. Earth* 12, 229–237.
- Sellwood, B.W., 1971. The genesis of some sideritic beds in the Yorkshire Lias (England). *J. Sediment. Res.* 41, 854–858.
- Sellwood, B.W., Jenkyns, H.C., 1975. Basins and swells and the evolution of an epeiric sea (Pliensbachian–Bajocian of Great Britain). *J. Geol. Soc. Lond.* 131, 373–388.
- Simms, M.J., Chidlaw, N., Morton, N., Page, K.N., 2004. *British Lower Jurassic Stratigraphy*. Geological Conservation Review Series, vol. 30. Joint Nature Conservation Committee, Peterborough. ISBN 1-86107-495-6. 458 pages, illustrations, A4 hardback.
- Sinninghe Damsté, J.S., Kenig, F., Koopmans, M.P., Koster, J., Schouten, S., Hayes, J.M., De Leeuw, J.W., 1995. Evidence for gammacerane as an indicator of water column stratification. *Geochim. Cosmochim. Acta* 59, 1895–1900.
- Suan, G., Mattioli, E., Pittet, B., Mailliot, S., Lécuyer, C., 2008. Evidence for major environmental perturbation prior to and during the Toarcian (Early Jurassic) oceanic anoxic event from the Lusitanian Basin, Portugal. *Paleoceanography* 23, PA1202. <https://doi.org/10.1029/2007PA001459>.

- Suan, G., Rulleau, L., Mattioli, E., Suchéras-Marx, B., Rousselle, B., Pittet, B., Vincent, P., Martin, J.E., Léna, A., Spangenberg, J.E., Föllmi, K.B., 2013. Palaeoenvironmental significance of Toarcian black shales and event deposits from southern Beaujolais, France. *Geol. Mag.* 150, 728–742.
- Suan, G., van de Schootbrugge, B., Adatte, T., Fiebig, J., Oschmann, W., 2015. Calibrating the magnitude of the Toarcian carbon cycle perturbation. *Paleoceanography* 30, PA2758. <https://doi.org/10.1002/2014PA002758>.
- Svensen, H., Planke, S., Chevallier, L., Malthe-Sorensen, A., Corfu, F., Jamtveit, B., 2007. Hydrothermal venting of greenhouse gases triggering Early Jurassic global warming. *Earth Planet. Sci. Lett.* 256, 554–566.
- Svensen, H., Corfu, F., Polteau, S., Hammer, Ø., Planke, S., 2012. Rapid magma emplacement in the Karoo Large Igneous Province. *Earth Planet. Sci. Lett.* 325–326, 1–9.
- Tappin, D.R., Chadwick, R.A., Jackson, A.A., Wingfield, R.T.R., Smith, N.J.P., 1994. Geology of Cardigan Bay and the Bristol Channel, United Kingdom Offshore Regional Report. British Geological Survey, HMSO. 107 pp.
- Them, T.R., Gill, B.C., Carruthers, A.H., Gröcke, D.R., Tulskey, E.T., Martindale, R.C., Poulton, T.P., Smith, P.L., 2017. High-resolution carbon isotope records of the Toarcian Oceanic Anoxic Event (Early Jurassic) from North America and implications for the global drivers of the Toarcian carbon cycle. *Earth Planet. Sci. Lett.* 459, 118–126.
- Thiry, M., 2000. Palaeoclimatic interpretation of clay minerals in marine deposits: an outlook from the continental origin. *Earth-Sci. Rev.* 2000, 201–221.
- Torsvik, T.H., Van der Voo, R., Preeden, U., Mac Niocaill, C., Steinberger, B., Doubrovine, P.V., van Hinsbergen, D.J.J., Domeier, M., Gaina, C., Tohver, E., Meert, J.G., McCausland, P.J.A., Cocks, L.R.M., 2012. Phanerozoic polar wander, palaeogeography and dynamics. *Earth-Sci. Rev.* 114, 325–368.
- Ullmann, C.V., Thibault, N., Ruhl, M., Hesselbo, S.P., Korte, C., 2014. Effect of a Jurassic oceanic anoxic event on belemnite ecology and evolution. *Proc. Natl. Acad. Sci.* 111, 10073–10076.
- van Bergen, P.F., Poole, I., 2002. Stable carbon isotopes of wood: a clue to palaeoclimate? *Palaeogeogr. Palaeoclimatol. Palaeoecol.* 182, 31–45.
- van de Schootbrugge, B., Bailey, T.R., Katz, M.E., Wright, J.D., Rosenthal, Y., Feist-Burkhardt, S., Falkowski, P.G., 2005. Early Jurassic climate change and the radiation of organic walled phytoplankton in the Tethys Sea. *Paleobiology* 31, 73–97.
- Wignall, P.B., Bond, D.P.G., Kuwahara, K., Kakuwa, Y., Newton, R.J., Poulton, S.W., 2010. An 80 million year oceanic redox history from Permian to Jurassic pelagic sediments of the Mino-Tamba terrane, SW Japan, and the origin of four mass extinctions. *Glob. Planet. Change* 71, 109–123.
- Wilkin, R.T., Barnes, H.L., Brantley, S.L., 1996. The size distribution of framboidal pyrite in modern sediments: an indicator of redox conditions. *Geochim. Cosmochim. Acta* 60, 3897–3912.
- Woodfine, R.G., Jenkyns, H.C., Sarti, M., Baroncini, F., Violante, C., 2008. The response of two Tethyan carbonate platforms to the early Toarcian (Jurassic) oceanic anoxic event: environmental change and differential subsidence. *Sedimentology* 55, 1011–1028.
- Woodland, A.W. (Ed.), 1971. The Llanbedr (Mochras Farm) Borehole. Institute of Geological Sciences, pp. 27–28. Report No. 71/18.
- Xu, W., Ruhl, M., Jenkyns, H.C., Hesselbo, S.P., Riding, J.B., Selby, D., Naafs, B.D.A., Weijers, J.W.H., Pancost, R.D., Tegelaar, E.W., Idiz, E.F., 2017. Carbon sequestration in an expanded lake system during the Toarcian Oceanic Anoxic Event. *Nat. Geosci.* 10, 129–134.